Geochemical behaviour of host phases for actinides and fission products in crystalline ceramic nuclear waste forms

GREGORY R. LUMPKIN[1,2], KATHERINE L. SMITH[2], RETO GIERÉ[3] & C. TERRY WILLIAMS[4]

[1]*Cambridge Centre for Ceramic Immobilisation, Department of Earth Sciences, University of Cambridge, Downing Street, Cambridge CB2 3EQ, UK (e-mail: gregl@esc.cam.ac.uk)*

[2]*Australian Nuclear Science and Technology Organisation, PMB 1, Menai, NSW 2234, Australia*

[3]*Department of Earth and Atmospheric Sciences, Purdue University, West Lafayette, IN 47907-1397, USA and Institut für Mineralogie, Petrologie und Geochemie, Universität Freiburg, Albertstrasse 23B, D-79104 Freiburg, Germany*

[4]*Department of Mineralogy, The Natural History Museum, Cromwell Road, London SW7 5BD, UK*

Abstract: A number of polyphase or single-phase ceramic waste forms have been considered as options for the disposal of nuclear waste in geological repositories. Of critical concern in the scientific evaluation of these materials is their performance in natural systems over long periods of time (e.g., 10^3 to 10^6 years). This paper gives an overview of the aqueous durability of the major titanate host phases for actinides (e.g., Th, U, Np, Pu, Cm) and important fission products (e.g., Sr and Cs) in alternative crystalline ceramic waste forms. These host phases are compared with reference to some basic acceptance criteria, including the long-term behaviour determined from studies of natural samples. The available data indicate that zirconolite and pyrochlore are excellent candidate host phases for actinides. These structures exhibit excellent aqueous durability, crystal chemical flexibility, high waste loadings, and well-known processing conditions. Although both pyrochlore and zirconolite become amorphous due to alpha-decay processes, the total volume swelling is only 5–6% and there is no significant effect of radiation damage on aqueous durability. Hollandite also appears to be an excellent candidate host phase for radioactive Cs isotopes. Brannerite and perovskite, on the other hand, are more prone to alteration in aqueous fluids and have a lower degree of chemical flexibility. With the exception of hollandite, many of the properties of these potential host phases have been confirmed through studies of natural samples.

The immobilization and long-term disposal of nuclear wastes is a world-wide issue and one of the greatest challenges facing modern society today. In the USA, for example, large amounts of high-level wastes (HLW) have been generated from the operation of commercial nuclear power stations and the nuclear weapons programme. The main sources of HLW are spent fuel from commercial nuclear power stations, liquid wastes from the reprocessing program of the 1960s, wastes generated from the production of nuclear weapons, and weapons-grade plutonium resulting from nuclear disarmament treaties between the USA and Russia. In 1994, approximately 400 000 cubic meters of HLW was stored in more than 200 underground tanks at the major United States Department of Energy (USDOE) sites (Ewing *et al.* 1995; Weber *et al.* 1998).

The current policy of the USA allows for the direct disposal of the spent fuel from commercial power generation, whereas most of the HLW from the defence programme is intended for immobilization using borosilicate glass. Borosilicate glass is also the currently accepted material for many countries that continue to reprocess their commercial spent fuel (e.g., England, France, Japan, and Russia). Nevertheless, a significant fraction of the existing 'legacy' wastes are characteristically very complex in physical

From: GIERÉ, R. & STILLE, P. (eds) 2004. *Energy, Waste, and the Environment: a Geochemical Perspective*. Geological Society, London, Special Publications, **236**, 89–111.
0305-8719/04/$15

form and chemical composition. These complex waste materials, together with scrap plutonium, and the fission products and actinides generated from the various partitioning strategies, may be better suited for existing or new types of high-performance crystalline waste forms or glass–ceramics (Donald *et al.* 1997; Trocellier 2000, 2001; Fillet *et al.* 2002, 2004).

In the existing strategy for HLW disposal using spent fuel and borosilicate glass, these HLW materials are part of a multibarrier concept relying heavily on the container, backfilling materials, and the repository itself for prevention of radionuclide migration into the environment. There are a number of alternative crystalline waste forms that may be capable of providing a much higher level of chemical durability as the best defence against radionuclide migration away from the repository. Some of these waste forms are illustrated in Table 1. Materials such as tailored ceramics (Harker 1988), the Synroc titanate waste forms (Fielding & White 1987; Ringwood *et al.* 1988), and their special purpose derivatives (e.g., pyrochlore, zirconolite, and hollandite) are reasonably well developed and have been the subject of extensive dissolution testing and radiation damage studies. Pyrochlore is the major component of Synroc-F, a polyphase ceramic designed for partially reprocessed nuclear fuel (Ball *et al.* 1989) and later appeared as the principle host phase for excess weapons Pu and U in a crystalline titanate ceramic form. Zirconolite has also been proposed as an ideal host phase for actinides due to a combination of crystal chemical flexibility and very high durability in aqueous fluids (Vance 1994). In view of the current 'partitioning' strategies for actinides and fission products, it has become apparent that hollandite may provide an excellent host material for separated radioactive Cs for similar reasons of crystal chemistry and durability (e.g., Kesson 1983; Cheary 1988).

As noted by Stewart *et al.* (2003), any existing or new high-performance waste form must meet several requirements in order to reach final consideration for use in a repository. These requirements are (1) a high level of durability in aqueous fluids, (2) crystal chemical flexibility allowing the material to incorporate impurity elements on crystallographic sites of the chosen host phases, (3) acceptable waste loadings, and (4) a reliable and cost-effective means of processing. In view of recent trends, one might be tempted to add radiation resistance as a fifth criterion. However, we prefer a more general statement: (5) the material must possess acceptable physical and mechanical properties including thermal behaviour, hardness, radiation damage induced swelling, cracking, and so on (Donald *et al.* 1997; Trocellier 2000; Stefanovsky *et al.*, 2004,

Table 1. *A selection of crystalline ceramic waste forms, applications, and mineralogy*

Waste form	Application	Mineralogy
Tailored ceramics	High Al SRP waste, 86 wt% loading	Magnetoplumbite, spinel, uraninite ± corundum, perovskite, pseudobrookite
	High Al RHO Purex SRP waste, 60 wt% loading	Magnetoplumbite, zirconolite, spinel, pseudobrookite, perovskite, rutile, loveringite
	SRP Composite HLW, 60 wt% loading	Magnetoplumbite, spinel, nepheline, uraninite, corundum
	SRP Composite HLW, 60 wt% loading	Nepheline, spinel, zirconolite, perovskite, murataite, magnetoplumbite
	Barnwell HLW, up to 57 wt% loading	Pyrochlore, perovskite, monazite, fluorite, intermetallic phases
Synroc-C	Purex type HLW from reprocessed spent fuel, 10–20 wt%	Ba–Cs–hollandite, perovskite, rutile, zirconolite, Al oxides, intermetallic phases
Synroc-C	Japanese type HLW from reprocessed spent fuel, 10–20 wt%	Ba–Cs–hollandite, perovskite, rutile, zirconolite, freudenbergite, loveringite, Al oxides, intermetallic phases
Synroc-D	US defence waste, 60–70 wt%	Zirconolite, perovskite, spinel, nepheline
Synroc-E	HLW from reprocessed spent fuel, 5–7 wt%	Rutile, Cs–hollandite, perovskite, zirconolite
Synroc-F	Conversion of spent fuel, 50 wt%	Pyrochlore, perovskite, uraninite ± hollandite
Pyrochlore	Pu, U, other ACTs, up to 35 wt%	Pyrochlore ± brannerite, baddeleyite, rutile
Zirconolite	Pu, U, other ACTs, up to 25 wt%	Zirconolite ± baddeleyite, rutile
Hollandite	Separated radioactive Cs, 5–10 wt% easily achieved	Ba–Cs–hollandite ± rutile

for details). Ultimately, it is the overall balance sheet that is important and there may be cases where a material that becomes amorphous due to radiation damage may excel in other areas and vice versa. Although studies of natural systems provide the only means of confirming the long-term behaviour of a given waste form phase, this concept is seldom considered at a level on par with the criteria listed above (see Crovisier *et al.*, 2004). In fact, such studies have closely paralleled the experimental research and development programmes over the past 30 years and extensive data sets now exist for many of the candidate waste form phases (Lumpkin 2001). The purpose of this paper is to review the available data for the major crystalline titanate ceramics and their mineral analogues.

Geochemical alteration

Pyrochlore

The structure of pyrochlore is considered to be an anion-deficient derivative of the fluorite structure type with a doubled *a* cell parameter and change in space group from *Fm3m* to *Fd3m* (Subramanian *et al.* 1983; Chakoumakos 1984; Smith & Lumpkin 1993). Minerals of the pyrochlore group conform to the general formula $A_{2-m}B_2X_{6-w}Y_{1-n}\cdot pH_2O$, where A represents cations in eightfold coordination, B represents cations in sixfold coordination, and X and Y are anion sites. The basic structural element of pyrochlore is the framework of corner-sharing octahedra. Within this framework, continuous tunnels are arranged parallel to the <110> directions. Both the A-site cations and Y-site anions are located in these tunnels. In synthetic systems, some A-site cation exchange capacity has been demonstrated in defect pyrochlores, in which the values of *m* in the general formula can be quite large.

Natural pyrochlore typically crystallizes under magmatic conditions in granitic pegmatites, nepheline syenite pegmatites, and carbonatites (in both calcite- and dolomite-rich varieties). The composition of common pyrochlore usually approaches the stoichiometric form $(Na, Ca, REE, U)_2(Nb, Ta, Ti)_2O_6(F, OH, O)$, but the structure type is extremely flexible in terms of the sheer number of elements that can be incorporated, and is particularly amenable to the incorporation of actinides. Natural samples are known to contain up to 30 wt% UO_2, 9 wt% ThO_2, and 16 wt% REE_2O_3, an important consideration for the issue of nuclear criticality. However, as shown by the general formula, the crystal chemistry of pyrochlore is complicated by the potential for vacancies at the A-, X-, and Y-sites ($m = 0.0–1.7$, $w = 0.0–0.7$, and $n = 0.0–1.0$) and the incorporation of water molecules ($p = 0–2$) in the vacant tunnel sites. The total water content of the natural defect pyrochlores may be as high as 10–15 wt% H_2O (with speciation as both water molecules and OH groups).

Numerous investigations have demonstrated that the pyrochlore structure type is susceptible to alteration via reaction with aqueous fluids over a range of P–T–X conditions. These studies have been recently reviewed in detail by Lumpkin (2001) and will only be summarized briefly here. A number of authors have studied the behaviour of Nb- and Ta-rich pyrochlore group minerals in natural systems (Lumpkin *et al.* 1986; Wise & Černý 1990; Ohnenstetter & Piantone 1992; Lumpkin & Ewing 1992, 1995, 1996; Lumpkin & Mariano 1996; Wall *et al.* 1996; Williams *et al.* 1997; Chakhmouradian & Mitchell 1998; Lumpkin 1998; Nasraoui *et al.* 1999). These authors found that many samples of pyrochlore exhibit geochemical alteration effects under a range of P–T–X conditions from weathering environments to late-stage magmatic and hydrothermal conditions associated with igneous intrusions. The alteration patterns of pyrochlore group minerals generally follow the coupled substitution schemes listed below (where □ represents a vacancy):

$$^{A}\square^{Y}\square \longrightarrow {}^{A}Ca^{Y}O$$
$$^{A}Na^{Y}F \longrightarrow {}^{A}Ca^{Y}O$$
$$^{A}Na^{Y}OH \longrightarrow {}^{A}Ca^{Y}O$$
$$^{A}Na^{Y}F \longrightarrow {}^{A}\square^{Y}\square$$
$$^{A}Ca^{Y}O \longrightarrow {}^{A}\square^{Y}\square$$
$$^{A}Ca^{X}O \longrightarrow {}^{A}\square^{X}\square$$

From top to bottom, these exchange mechanisms generally reflect the changes that occur from high- to low-temperature environments, although the details vary with rock type and specific P–T–X conditions. At higher temperatures (~300–650 °C, <400 MPa) in highly evolved late-stage magmatic fluids, Ca enrichment is commonly observed (via the filling of vacancies and replacement of Na–F by Ca–O pairs). The main effect of alteration at moderate temperatures under hydrothermal conditions (~200–350 °C, <200 MPa) is the loss of Na and F, typically combined with some cation exchange for Sr, Ba, REE, and Fe to produce a hydrated pyrochlore near $AB_2O_6\cdot H_2O$ in stoichiometry. Additional removal of Na, F, Ca, and O may occur in low-temperature

hydrothermal or weathering environments. These defect pyrochlores tend to exhibit maximum numbers of A-site, Y-site, and X-site vacancies, maximum hydration levels, and may take up large cations such as K, Sr, Cs, Ba, Ce, and Pb in certain environments. An example of this type of alteration is shown in Figures 1 and 2. Note that the alteration effects illustrated here are largely confined to the Na–Ca–F pyrochlores, (Na,Ca, $REE,U)_2(Nb,Ta,Ti)_2O_6(F,OH,O)$, in which the REE and U contents usually remain unchanged (e.g., Lumpkin & Ewing 1992, 1996). Under extreme lateritic weathering, fragmentation and subsequent dissolution of pyrochlore can occur, with precipitation of Nb and other B-site cations in submicron amorphous material consisting predominantly of Fe, Al, and P, with variable Si, Ca, and Ti. The available results suggest that Th is retained within micron-size secondary phases, whereas U is relatively mobile and may be released from U-rich zones in altered pyrochlore crystals (Wall *et al.* 1999).

A variety of alteration effects have been observed in completely metamict Ti- and U-rich pyrochlores. In the samples from Adamello, Italy, the pyrochlore occurs as overgrowths on zoned zirconolite grains and contains 29–34 wt% UO_2. Electron microscopy and microanalytical work has revealed that these pyrochlore samples have

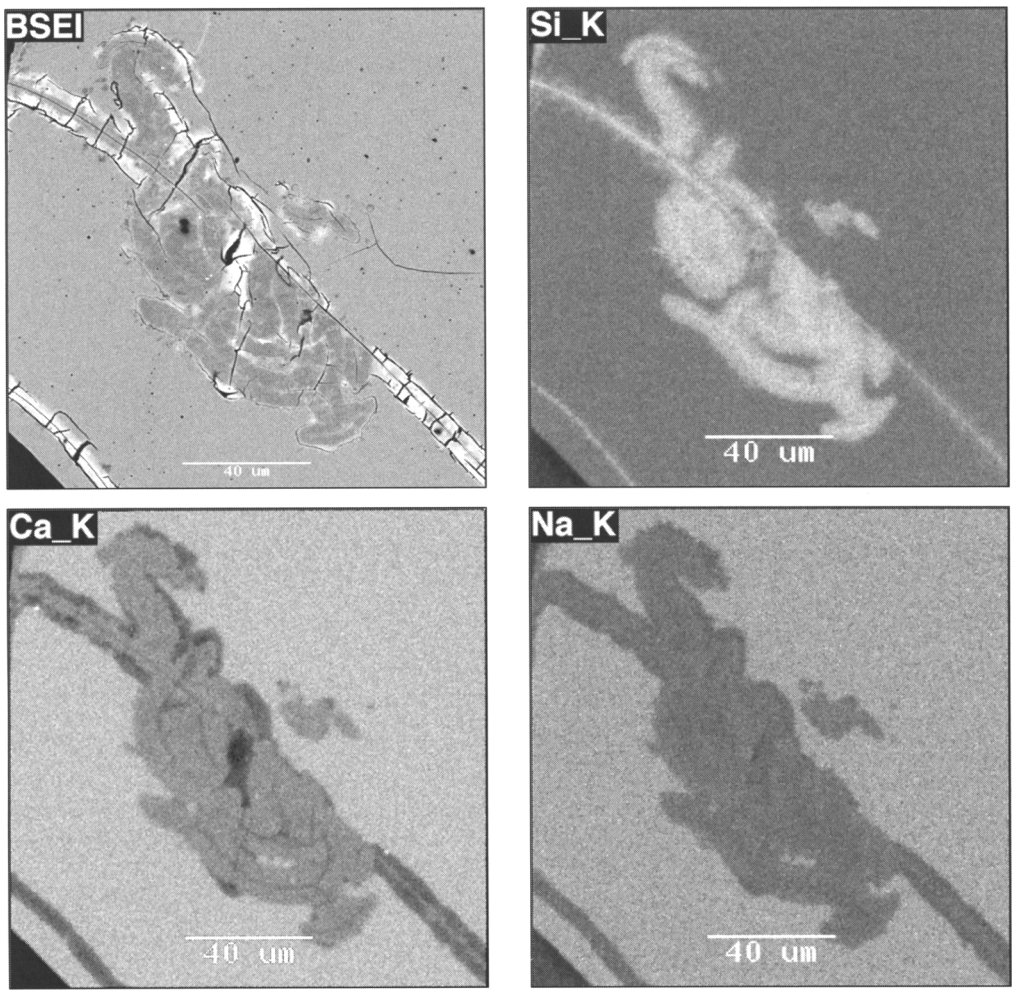

Fig. 1. SEM backscattered electron image, Si X-ray map, Ca X-ray map, and Na X-ray map of alteration in pyrochlore from Vishnevogorskii, Russia. Note the loss of Na and Ca and incorporation of Si along cracks and the dark area near the middle of the backscattered image.

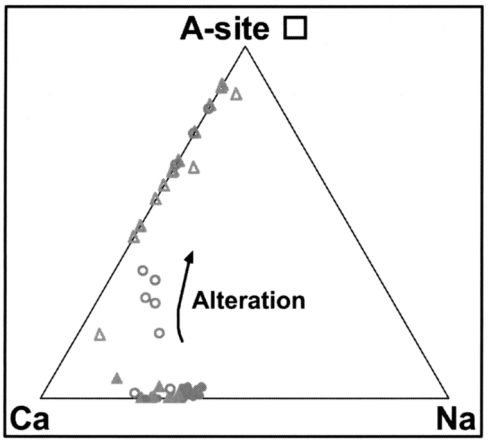

Fig. 2. Triangular plot of Ca, Na, and A-site vacancies in pyrochlore from Vishnevogorskii calculated from structural formulae normalized to two B-site cations. Compositions of primary pyrochlore plot near the Ca–Na join (solid symbols). Compositions of the altered areas move toward the Ca-vacancy join, then along this join toward the top of the triangle.

only suffered a minor late-stage hydration event as evidenced by lower backscattered electron image contrast around the rims of the grains. Results of this study demonstrate retention of U and Th for time periods of 40 Ma, even though the cumulative total alpha-decay dose is on the order of 3 to 4×10^{16} α mg^{-1} (Lumpkin *et al.* 1999). In two samples from Bancroft, Ontario, Canada, Lumpkin & Ewing (1996) had previously concluded that the major result of alteration was hydration, with only minor changes in elemental composition, apart from the precipitation of galena due to mobility of radiogenic Pb. In contrast to these examples, the Ti- and U-rich pyrochlores from Madagascar exhibit a range of alteration effects beginning with a relatively low temperature style of alteration that initially proceeds by removal of Na, Ca, and F as shown in the list above. The alteration is usually accompanied by hydration together with minor increases in Al, K, Mn, Fe, Sr, and Ba. At this stage, U and Th remain relatively unaffected by the alteration process (stage 1). If the Ca content drops below about 0.2–0.3 atoms per formula unit, these Ti-rich pyrochlores exhibit various levels of recrystallization to liandratite + uranpyrochlore + rutile (or anatase) and partial dehydration (stage 2). This may be accompanied by loss of up to 20–30% of the original amount of U and local redistribution of the radiogenic Pb.

The effect of radiation damage on the alteration of 440 Ma old pyrochlore from Mozambique has been studied by Gieré *et al.* (2000, 2001). These pyrochlore crystals exhibit distinctive chemical zoning, characterized by a U-free core and a U-rich rim (up to 17 wt% UO_2). Following uplift and cooling, groundwater penetrated these fractured crystals and led to the deposition of clay minerals along both fractures and cleavage planes. This low-temperature process also led to chemical alteration of the pyrochlore, but only within the zone of the U-rich rim. During this alteration, which is the result from exposure to tropical conditions, Na, Ca, and F were removed from the pyrochlore, leading to increased A-site vacancies (up to about 1.8 A-site vacancies per formula unit). The alteration also led to localized redistribution of radiogenic Pb and to hydration, but U remained immobile. The low-temperature alteration effects are only observed in the U-rich rim, which is largely amorphous and characterized by abundant microfractures, suggesting that the susceptibility of pyrochlore to low-temperature alteration is enhanced by the microstructural damage caused by the α-decay of U (also see Ohnenstetter & Piantone 1992).

Zirconolite

The structure of zirconolite (Smith & Lumpkin 1993) is also considered to be an anion-deficient derivative of the fluorite structure type. The structure can be viewed as a volumetrically condensed, layered version of pyrochlore with reduced symmetry and several polytypic forms (monoclinic 2M or 4M, both with space group $C2/c$; orthorhombic 3O with space group *Acam*, hexagonal 3T with space group $P3_121$). The chemical composition of zirconolite 2M corresponds to $CaZrTi_2O_7$, but in nature it typically deviates from this end-member composition due to extensive substitution of REE, Th, and U for Ca and Nb, Fe, and Mg for Ti (Gieré *et al.* 1998; Bellatreccia *et al.* 1999). Zirconolite may incorporate up to 24 wt% UO_2, 22 wt% ThO_2, and 32 wt% REE_2O_3 in natural systems. In natural samples Zr is subject to only limited substitution by other elements (e.g., minor amounts of Y, REE, U, and Ti). Experimental work has shown that extensive substitution of REE, Th, and U generally results in a polytypic phase transformation from monoclinic 2M to trigonal 3T or from monoclinic 2M to monoclinic 4M. It is often difficult to determine the polytype of natural zirconolite due to extensive radiation damage; however, the polytypes 2M, 3O, and 3T are known from a few samples with low alpha-decay dose (Sinclair & Eggleton 1982; Mazzi & Munno 1983; Bellatreccia *et al.* 2002).

Isotopic age dating work by Oversby & Ringwood (1981) and electron microscopy studies by Ewing *et al.* (1982) demonstrate that zirconolite remained a closed system with respect to U, Th, and Pb for up to 650 Ma with little, if any, evidence for geochemical alteration. Lumpkin *et al.* (1994), Gieré *et al.* (1994), and Hart *et al.* (1996) have described the alteration of metamict zirconolite from the 2060 Ma carbonatite complex of Phalaborwa, South Africa, in somewhat greater detail. Electron microprobe analyses, element mapping, and backscattered electron images demonstrate that the alteration is localized along cracks and resulted in the incorporation of Si and loss of Ti, Ca, and Fe. However, in these samples the REE, Th, and U contents remained relatively constant across the alteration zones. Radiogenic Pb appears to have been mobile and precipitated mainly within the altered areas as galena (PbS), similar to observations reported by Lumpkin & Ewing (1996) for metamict U- and Ti-rich pyrochlores.

At higher temperature and pressure in magmatic, hydrothermal, or metamorphic systems, zirconolite may be altered by dissolution–reprecipitation or replacement mechanisms. Gieré & Williams (1992) have described zoned zirconolites from Adamello, Italy, which exhibit corrosion and replacement by a new generation of zirconolite together with loss of Th and U to a hydrothermal fluid. Importantly, a thermodynamic analysis of the mineral assemblages was performed in this work and indicated that the zirconolite crystallization and corrosion occurred at 500–600 °C in a reducing hydrothermal fluid rich in H_2S, HCl, HF, and P and relatively poor in CO_2. Pan (1997) has also described the breakdown of zirconolite to a new mineral assemblage consisting of zircon, sphene, and rutile in metamorphosed (~600 °C) ferromagnesian silicate rocks at Manitouwadge, Canada. This reaction can be expressed as follows (modified slightly from Pan 1997):

$$CaZrTi_2O_7 + 2SiO_2 = ZrSiO_4 + CaTiSiO_5 + TiO_2$$

Bulakh *et al.* (1998) and Williams *et al.* (2001) have reported on the alteration of zirconolite from carbonatites. In these examples, the zirconolite has been replaced along cracks and within micron-sized domains by an unidentified Ba–Ti–Zr–Nb–ACT silicate phase, suggesting that zirconolite may not be stable in the presence of hydrothermal fluids rich in Si. Figure 3 presents an example of this type of alteration, where one may see additional evidence for enhanced alteration along zones enriched in Th and U. In contrast to pyrochlore, however, where complete breakdown of this mineral can occur in extreme tropical lateritic weathering environments (see above), zirconolite appears relatively resistant to dissolution, with only minor dissolution features occurring at the margins (Williams *et al.* 2001).

Brannerite

Brannerite, ideally UTi_2O_6, has a crystal structure based on a distorted array of hexagonal close packed oxygens. The structure is monoclinic, space group $C2/m$, and consists of layers of Ti octahedra connected by columns of U octahedra (Szymański & Scott 1982). Natural and synthetic brannerites can incorporate substantial amounts of Ca, REE, Th, and other elements. In both cases, the incorporation of lower valence elements on the A-site may be charge balanced by oxidation of some U^{4+} to U^{5+} and/or U^{6+} ions (Vance *et al.* 2000). Lumpkin *et al.* (2000) have examined brannerite samples from different localities by SEM-EDX, showing that the unaltered areas of the samples contain up to 7 wt% CaO, 8 wt% REE_2O_3, 7 wt% PbO, and 15 wt% ThO_2. Low but variable amounts of Al_2O_3, SiO_2, MnO, FeO, NiO, and Nb_2O_5 were also found in these samples.

Electron microscopy studies show that most natural brannerites with ages greater than about 10 Ma are fully amorphous due to alpha-decay damage and are commonly altered by natural aqueous fluids (Lumpkin 2001). Alteration usually occurs around the rim of the brannerite or along cracks (Fig. 4*a*), and may involve the formation secondary such as anatase, galena, and thorite. As reported for pyrochlore and zirconolite, the galena may precipitate due to the combined effects of radiogenic Pb migration and the presence of S species in the aqueous fluid. Altered brannerite typically loses U and the concentration may decrease to approximately 1 wt% UO_2 in the most heavily altered areas (Fig. 5). The loss of U may be compensated in part by the incorporation of up to 18 wt% SiO_2 and 16 wt% FeO, together with significant amounts of P_2O_5, As_2O_5, and Al_2O_3 in certain examples. In some cases, the associated rock or mineral matrix surrounding the brannerite may be highly fractured, providing pathways for the migration of U, evidenced by the precipitation of secondary U minerals (Lumpkin *et al.* 2000). An example of this process is illustrated in Fig. 4*b*.

Hollandite

The crystal structure of hollandite, $A_{1.1-1.7}B_8O_{16}$, is similar to that of rutile and consists of edge-

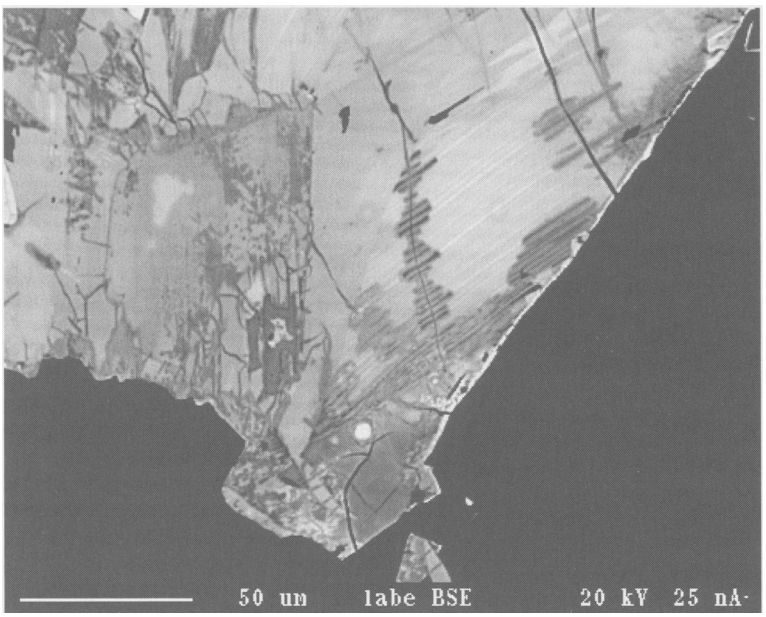

Fig. 3. SEM backscattered electron image of alteration in zirconolite from the Afrikanda alkaline complex, Kola Peninsula, Russia. This crystal exhibits complex magmatic zoning, late-stage replacement by an unknown Ba–Zr–Ti–silicate phase, and preferential alteration along cracks and Th–U-rich zones.

sharing chains of octahedra connected via corner sharing to form a three-dimensional framework. Hollandite, however, has two octahedral chains connected by edge-sharing instead of the single chain found in rutile, resulting in a rather large 2×2 tunnel capable of accommodating large A-site cations like K, Rb, Cs, and Ba (Kesson & White 1986*a*, *b*; Cheary 1987). These cations exhibit various ordering sequences over the available tunnel sites, commonly resulting in superlattice peaks in X-ray or electron diffraction patterns. In general, the superlattice is incommensurate with the sublattice as defined by the octahedral cation repeat distance, but may be commensurate for A-site occupancy values of 1.200, 1.333, and 1.500 atoms per formula unit. The space group is typically $I4/m$ or $C2/m$ depending upon the A/B cation radius ratio. Numerous synthetic samples have been produced with Ti, Mn, Mo, noble metals, or Sn as the most common major elements and with Mg, Al, V, Fe, Co, Ni, Zn, and Sb, among others, as minor elements on the B-site. The composition of hollandite in titanate-based waste forms is generally given as $(Ba_x Cs_y)[(Ti,Al)^{3+}_{2x+y}Ti^{4+}_{8-2x-y}]O_{16}$ in which charge compensation for Ba and Cs is usually provided by Al or Ti^{3+} (Myhra *et al.* 1988*a*; Carter *et al.* 2002; Bart *et al.* 2003).

In natural samples (cryptomelane group), typical B-site cations are Ti, V, Cr, Fe, Mn^{2+}, and especially tetravalent Mn^{4+}. The closest natural analogue for synthetic titanium hollandite is the mineral priderite, which occurs in the leucite lamproites of Western Australia and elsewhere and has a composition of approximately $(Ba,K)_{1.2-1.6}[Ti,Fe,Mg]_8O_{16}$ (Sinclair & McLaughlin 1982; Post *et al.* 1982). Unfortunately, priderite is a relatively rare mineral and there have been no detailed studies of the alteration of this phase in natural systems.

Perovskite

Perovskite is an ABX_3 structure type based around a framework of corner-sharing, octahedral B-site cations. The large A-site cations occupy the center of a large cavity formed by eight B-site octahedra and are coordinated to 12 oxygens in the ideal cubic structure. Most perovskites are distorted via octahedral tilting and generally have lower symmetry. In nature, only near end-member $SrTiO_3$ is cubic; most other compositions are orthorhombic (Mitchell 1996). The major A-site cations in natural perovskites are Na, Ca, Sr, and REE, with minor amounts of K, Ba, and U. The concentration of Th is usually low, but may reach levels as high as 18 wt% ThO_2 in certain alkaline rocks (Mitchell & Chakhmouradian 1998*a*). The B-site of natural perovskite is occupied predominantly by Ti, Fe, and Nb, together

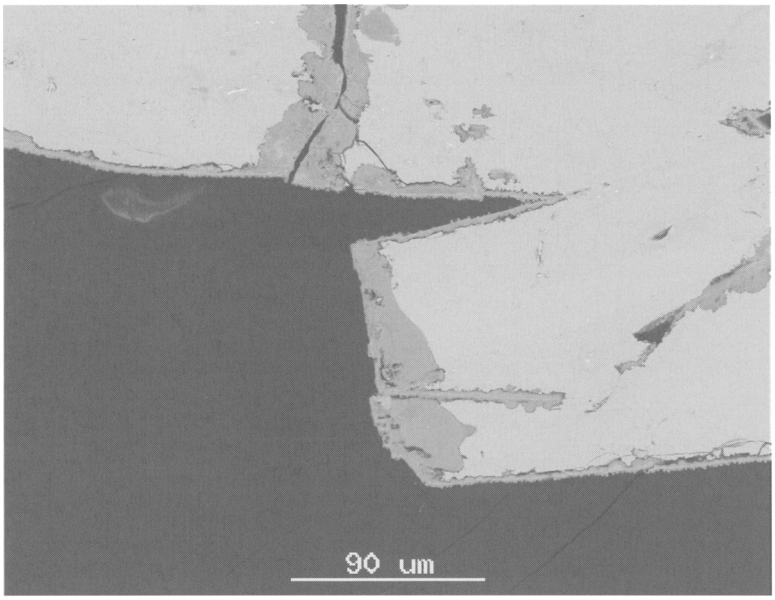

(a)

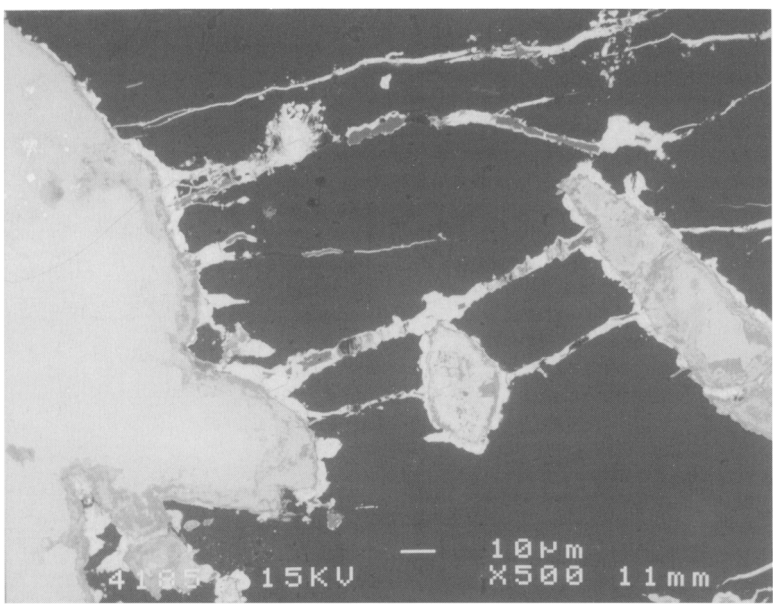

(b)

Fig. 4. SEM backscattered electron images of alteration in natural brannerite: (**a**) Part of a large brannerite specimen showing minor alteration around the rim of the crystal and along fractures extending into the interior; (**b**) Brannerite crystals showing extensive alteration along their rims, together with the presence of U-rich phases along cracks in the host rock.

with minor amounts of Mg, Al, Zr, and Ta, depending on bulk rock chemistry and mineralogy.

In low-temperature environments, perovskite commonly breaks down to one or more polymorphs of TiO_2, in the process releasing Ca and possibly other elements into the aqueous fluid. This is well illustrated by the alteration of perovskite to anatase, cerianite, monazite, and

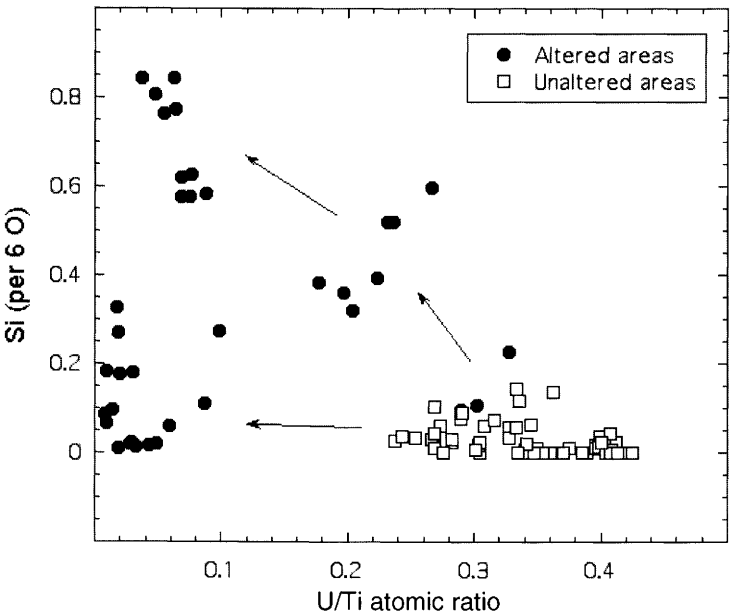

Fig. 5. Scatter plot showing the number of Si atoms per formula unit and the U/Ti atomic ratio in a suite of natural brannerite samples, (□, unaltered areas; ●, altered areas). In unaltered brannerite, the U/Ti ratio lies below the ideal value of 0.5 due to extensive substitution of Th, Ca, and minor REEs for U on the A-site.

crandallite group minerals during severe weathering of carbonatites in Brazil (Mariano 1989). Using electron microscopy, Banfield & Veblen (1992) have proposed that the perovskite–anatase reaction mechanism involves 'topotactic inheritance' of layers of the perovskite Ti–O framework. In hydrothermal systems, Mitchell & Chakhmouradian (1998*b*) have described the alteration of perovskite to kassite, anatase, titanite, calcite, and ilmenite in the presence of a CO_2- and SiO_2-rich fluid phase at temperatures of 250–600 °C in alkaline rocks. In general, the results reported above are consistent with the thermodynamic properties of perovskite and related minerals. Nesbitt *et al.* (1981) have shown that perovskite is unstable with respect to sphene, rutile, calcite, and quartz in many hydrothermal fluids and ground waters at 25–300 °C.

Na-bearing perovskite, or loparite (ideally $Na_{0.5}REE_{0.5}TiO_3$), is also subject to hydrothermal alteration in alkaline igneous rocks (Lumpkin *et al.* 1998; Chakhmouradian *et al.* 1999). The primary result of this alteration is removal of Na from the original perovskite, producing a phase which is now amorphous ('metaloparite') due to radiation damage and has a composition of approximately $REETi_2O_{6-x}(OH,F)_x \cdot H_2O$. It is entirely possible that this amorphous phase was originally lucasite, a mineral that is isostructural with kassite, $CaTi_2O_4(OH)_2 \cdot H_2O$. The simplified reaction relationships for perovskite, kassite, and lucasite are:

$$2H^+ + H_2O + 2CaTiO_3 = CaTi_2O_4(OH)_2 \cdot H_2O + Ca^{2+}$$

$$H^+ + H_2O + 2Na_{0.5}REE_{0.5}TiO_3 = REETi_2O_5(OH) \cdot H_2O + Na^+$$

In both cases, the replacement product is usually reported as having a distinctly fibrous or prismatic morphology. The higher level of radiation damage in metaloparite (lucasite?) could be due to a difference in the critical amorphization dose of loparite and the alteration product, provided that the alteration event occurred soon after crystallization of the loparite. For example, Smith *et al.* (1998) and Lumpkin *et al.* (1998) have shown that the critical amorphization dose of perovskite structure types may be as much as a factor of five greater than the critical dose of other Nb–Ta–Ti minerals (e.g., pyrochlore and zirconolite).

Perovskites also exhibit reaction relationships with phosphate minerals and exotic alkali–titanium–silicate minerals under late-stage magmatic conditions. In a systematic study of loparite mineral chemistry in the Lovozero alkaline complex, Russia, Kogarko *et al.* (2002) have

identified several reactions between loparite and a late-stage alkaline melt, where loparite was corroded and replaced by apatite, monazite, and the rare minerals lamprophyllite, lomonosovite, mosandrite, nenadkevichite, steenstrupine, and vitusite. During this stage of the evolution of the Lovozero peralkaline magma, concentrations of volatile components (F, H_2O) and alkalis reached very high levels, and reacted with loparite.

Experimental data

Polyphase ceramics

The basic dissolution tests carried out on polyphase Synroc formulations have been carried out in the temperature range 25–200 °C and in deionized water, following the standard MCC-1 and MCC-2 procedures, with periodic replacement of the aqueous fluid. Some additional tests have been performed using carbonate, saline, or silicate solutions instead of deionized water. Much of the early work on the polyphase ceramics, including the effects of composition and processing parameters on elemental release rates, has been reviewed by Ringwood *et al.* (1988) and will not be repeated in detail here. The release rates of soluble elements like Al, Ca, Sr, Mo, Cs, and Ba exhibit a non-linear decrease with time, typically from 10^{-1} g/m^2/d after one day to 10^{-3} g/m^2/d or lower after about 90 days at temperatures of 70–100 °C. Release rates of the rare earth elements are about an order of magnitude lower than the soluble elements and Ti and Zr are lower still, often reaching detection limits within a few days. Experiments performed at 90 °C reveal that the dissolution of Synroc-C has a weak dependence on pH, possibly with a shallow minimum near pH = 7. Over a temperature range of 45–300 °C, experiments indicate an increase in release rates by a factor of 25 and activation energies in the range 15–30 kJ/mol.

In subsequent work, Smith *et al.* (1991) showed that release rates of Cs, Mo, and Sr decrease rapidly with time in deionized water at 150 °C, reaching values below 10^{-3} g/m^2/d after 336 days. The release rates are lower by a factor of about 2–5 for experiments performed at 70 °C in deionized water. Interestingly, experiments were also run at 70 °C in bicarbonate and silicate solutions, and the release rates for Cs and Mo were lower still, a clear indication of the possible effects of real aqueous fluids. Further analysis of the data by Smith *et al.* (1992) showed that Al and Mo possessed the highest release rates in water at 150 °C, with about 0.1% of the original amount of these elements lost after 532 days. By way of comparison, about 0.06–0.07% Ca and Sr, 0.02–0.05% Ce and Nd, and 0.01–0.03% of the Cs and Ba were released after 532 days of testing. The chemical data are consistent with the maximum alteration depths observed by electron microscopy: 0.5 μm for intermetallic alloys, 0.3 μm for Al-rich phases, and 0.2 μm for perovskite. Using data for total mass loss, Smith *et al.* (1992) determined that the average alteration rate of Synroc is approximately 10^{-1} nm/d. It is possible to estimate the alteration depths of some of the phases in Synroc-C from elemental release rate data. This is illustrated in Fig. 6, where the cumulative alteration depth is plotted against time for two different temperatures. These results indicate that there is a significant increase in the alteration depth after increasing the temperature from 70 °C to 150 °C in pure water. The estimated alteration depths after 1 year at 150 °C are 350 nm for Al-rich oxides, 160 nm for perovskite, and 13 nm for hollandite (Fig. 6*b*) and are in good agreement with surface SEM and cross-sectional TEM observations (Smith *et al.* 1992).

At temperatures below 100 °C the major alteration product on the surface of Synroc consists of an amorphous or poorly crystalline Ti–O–H film derived mainly from the dissolution of perovskite (Murakami 1985; Kastrissios *et al.* 1987; Myhra *et al.* 1988*b*, 1988*c*; Solomah & Matzke 1989; Lumpkin *et al.* 1991, 1995; Smith *et al.* 1997*a*). Some dissolution of Mo-rich intermetallic particles is also observed at this temperature. Electron microscope observations made following experiments at 150 °C clearly reveal the alteration of perovskite to anatase + brookite, oxidative dissolution of intermetallic phases, dissolution of minor Al-rich phases, and the presence of scattered TiO_2 crystals on hollandite. Interestingly, monazite has also been observed as a secondary alteration product at 150 °C, incorporating REEs from perovskite and P from dissolving intermetallic grains. Other secondary phases at this temperature include at least two Al–O–H phases and a poorly crystalline Fe–O–H material (Lumpkin *et al.* 1995). Using cross-sectional TEM methods to examine the interface between perovskite and secondary TiO_2 phases, Smith *et al.* (1997*a*) have recently suggested that there may be a thin zone in the upper surface of the perovskite, approximately 40 nm thick, which is depleted in Ca and Sr.

Additional work has been carried out on the behaviour of actinides in Synroc-type ceramics (Ringwood *et al.* 1988; Reeve *et al.* 1989; Hart *et al.* 1992; Smith *et al.* 1996; 1997*b*).

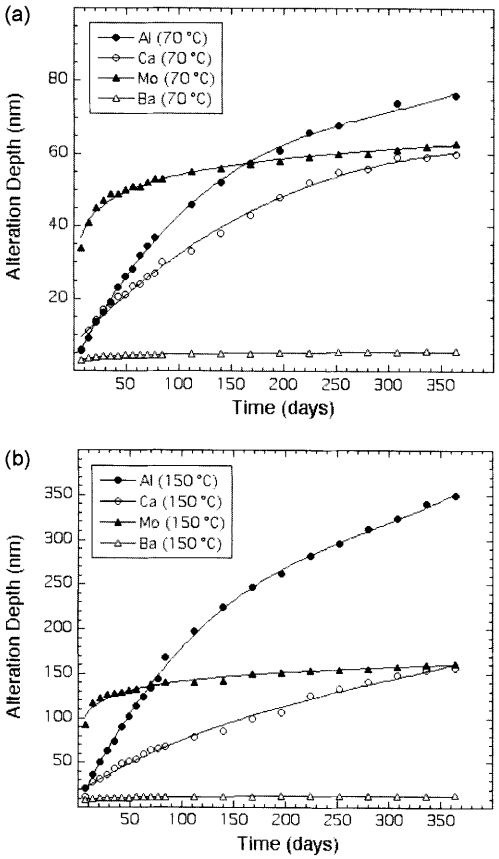

Fig. 6. Plots of the cumulative alteration depth versus time for Synroc-C in deionized water at 70 °C (**a**) and 150 °C (**b**). These plots use Al, Ca, Mo, and Ba as indicator elements for the alteration depth of Al-rich oxide phases, perovskite, intermetallic phases, and hollandite, respectively.

Importantly, the early studies summarized by Ringwood *et al.* (1988) suggested that the release rates of the actinides are approximately two orders of magnitude lower than the more soluble elements such as Ca, Sr, Mo, Cs, and Ba. This has been generally confirmed by Reeve *et al.* (1989), who report release rates of less than 10^{-4} g/m^2/d for ^{237}Np and less than 10^{-5} g/m^2/d for ^{239}Pu, ^{241}Am, and ^{244}Cm in short-term tests (less than 60 days). For experiments performed in buffered solutions of pH = 2–10 at 70 °C using Synroc containing Pu, Np, and Am, Hart *et al.* (1992) have used the EQ3/6 code to demonstrate that the solubility of Pu controls the behaviour in all experiments except for pH = 2. The solubility limits of Am and Np were not exceeded under any of the experimental conditions. The Pu and Np release rates decrease from a maximum of 10^{-3} g/m^2/d down to approximately 10^{-6} g/m^2/d after more than 2000 days in pure water at 70 °C (Smith *et al.* 1996, 1997*b*). For short-term tests, the results of Smith *et al.* (1997*b*) suggest that the Pu release rate increases by about one order of magnitude in silicate and carbonate solutions. Although surface characterization of the samples tested for long periods of time revealed the presence of abundant secondary phases (anatase, brookite, Fe-oxides, etc.), actinide elements were not detected (<0.2 wt%) within these alteration products.

The alteration of several titanate ceramics in pure water at 90 °C has been investigated by Leturcq *et al.* (2001). These experiments were performed under conditions of high surface area to volume ratio and lasted for over one year without replacement of the solution. Starting materials included melted Synroc-like materials and hot pressed Synroc-C. This study reported the normalized elemental mass losses, defined by the equation:

$$NL(i) = (C_i \times 1000)/(W_i \times S/V)$$

where C_i is the steady-state concentration in ppb of element i in solution, W_i is the weight percentage of element i in the starting material, S is the surface area of the specimen, and V is the volume of the liquid. Results demonstrate that steady-state concentrations were obtained after several days in solution. Normalized mass losses were typically between 10^{-1} and 10^{-4} g/m^2 for relatively soluble elements (Al, Ca, Mo, Sr, Cs, Ba) and between 10^{-4} and 10^{-7} g/m^2 for the less soluble elements (Ti, Zr, REEs). Thermodynamic calculations suggested that the 'cessation of alteration' is not explained by the solubility limits of the primary phases in the ceramics. The results appear to be consistent with the development of a layer of secondary material (Ti–Zr hydroxides) on the surface of the ceramic that retards the alteration process after a short period of time. The estimated thickness of this layer is about 3–5 nm, but unfortunately this thickness was stated as being less than the sensitivity of the characterization methods available to the authors (Leturcq *et al.* 2001).

In an important study of accelerated radiation damage effects in polyphase Synroc samples doped with ^{244}Cm, Mitamura *et al.* (1992, 1994) studied the behaviour of Mo, Sr, Ca, Cs, Ba, and Cm for up to 56 days in distilled water at 90 °C. These ceramics were doped with either Na-free simulated Purex waste (PW-4b) or simulated waste containing 1.65 wt% Na_2O (e.g., JW-A type). We should note here that the

two different waste streams lead to a real difference in the physical and chemical response to radiation damage. Up to the maximum dose achieved during this study (1.3×10^{15} α/mg), the PW-4b samples showed a consistent decrease in density with increasing dose. A single specimen loaded with JW-A type waste, however, showed a significant change in the dose–density behaviour at a dose of 8.5×10^{14} α/mg related to the onset of cracking (see fig. 5 in Mitamura *et al.* 1994). For the longest testing period, the release rates of Ca and Sr in the PW-4b samples were within error of one another and increased by less than a factor of 10 with increasing dose, from approximately 3×10^{-4} g/m^2/d to 2×10^{-3} g/m^2/d. The fact that Ca and Sr are released at approximately the same rate points to perovskite as the major source of these elements in solution, even though the damage rate of zirconolite appears to be much higher than that of perovskite according to the X-ray diffraction results.

Pyrochlore ceramics

A variety of pyrochlore ceramics have been studied using flow-through experiments in pH buffered solutions and a range of temperatures below 100 °C (Shoup *et al.* 1997; Icenhower *et al.* 2000; Roberts *et al.* 2000; Zhang *et al.* 2001*a*, *b*). Shoup *et al.* (1997) examined the behaviour of a pyrochlore ceramic, $Er_{1.78}Ce_{0.22}Ti_2O_7$, in three different aqueous fluids: WIPP type brine, 0.1 M NaCl, and 0.1 M HCl at 50 °C. All elements were below detection limits in the NaCl solution and only Er was detected at a level of 10 ppm in the WIPP brine. For acidic conditions, the authors reported 1375 ppm Er, 150 ppm Ce, and only 3 ppm Ti in solution. The Er/Ce ratio in solution is very close to that of the starting material; however, the measured amount of Ti in solution is well below the level of Er and Ce, possibly due to precipitation of secondary phases on the surface.

Icenhower *et al.* (2000) investigated $Gd_2Ti_2O_7$ and $Lu_2Ti_2O_7$ monoliths and $(Ca,Gd,Ce,Hf)_2(Ti,Mo)_2O_7$ powders at 90 °C and pH = 2–12. Release rates for Gd, Ce, and Ti at pH = 2 were approximately $1–4 \times 10^{-3}$ g/m^2/d and $4–7 \times 10^{-4}$ g/m^2/d for the $Gd_2Ti_2O_7$ and $Lu_2Ti_2O_7$ monoliths, respectively. The releases were essentially the same within experimental error. Experiments with the more complex sample in powdered form yielded release rates of $6–9 \times 10^{-5}$ g/m^2/d for Gd and Ce using a flow rate of 2 mL/d. Using a higher flow rate of 10 mL/d caused higher release rates of $2–4 \times 10^{-5}$ g/m^2/d. Release rates for all of the samples approached steady-state conditions after about 90 days. The release of Mo was used to monitor the dissolution of $(Ca,Gd,Ce,Hf)_2(Ti,Mo)_2O_7$ in neutral to basic solutions. Near steady-state Mo concentrations (0–4 ppb range) yield apparent dissolution rates of $2–6 \times 10^{-5}$ g/m^2/d for both samples at pH = 6–8 and flow rate = 2 mL/d. In total, the results for $(Ca,Gd,Ce,Hf)_2(Ti,Mo)_2O_7$ indicate a weak pH dependence with a minimum at pH = 7. Similar pyrochlore-rich ceramics were studied by Hart *et al.* (2000), who showed that the release rate of Pu dropped from approximately 10^{-3} g/m^2/d to 10^{-5} g/m^2/d or less after nearly one year in pure water at 90 °C (Fig. 7). The release rates of U and Gd in these experiments were higher than Pu by factors of about 10 and 100, respectively.

The kinetics of U release from a pyrochlore, $(Ca,Gd,Ce,Hf,U)_2Ti_2O_7$, containing 24 wt% UO_2 has been investigated by Roberts *et al.* (2000) and Zhang *et al.* (2001*b*). Although the results of these two studies differ in detail, they both report that the pH dependence follows a shallow V-shaped pattern with a minimum near neutral pH (Fig. 8). The activation energy (E_a) for the release of U ranges from about 3 to 20 kcal/mol below the minimum pH and from 3 to 12 kcal/mol above the minimum pH value. The release rates for U, converted from the limiting rate constants given by Zhang *et al.* (2001*b*), range from 6×10^{-7} g/m^2/d to 7×10^{-5} g/m^2/d for all experimental conditions (e.g., T = 25–75 °C and pH = 2–12).

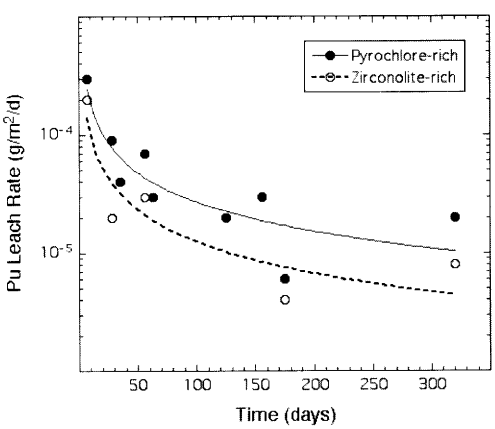

Fig. 7. Plot of the Pu leach rate as a function of time for pyrochlore- and zirconolite-rich LLNL-type waste forms in experiments performed at 90 °C in pure water (after Hart *et al.* 2000). Power law curve fits illustrate the normal trends for these materials: initial rapid decrease in leach rates followed by slower release rates, which decrease to 10^{-5} g/m^2/d or less after time periods of several months to one year.

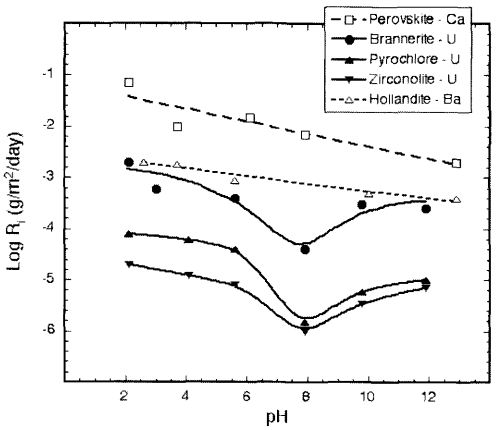

Fig. 8. Plots showing the dependence of the elemental release rate on pH for U in brannerite, pyrochlore, and zirconolite at 75 °C (after Zhang *et al.* 2001*b*). Also shown are data for Ca in perovskite and Ba in hollandite (after McGlinn *et al.* 1995; Carter *et al.* 2002). Linear fits are shown for perovskite and hollandite, but the other curves are weighted fits used to illustrate the trends.

Weber and co-workers were among the first investigators to conduct dissolution tests on single-phase pyrochlore samples ($Gd_2Ti_2O_7$) doped with ^{244}Cm (Weber *et al.* 1986). In this work, the dissolution tests were limited to annealed, fully crystalline samples and fully amorphous samples and were exercised at 90 °C in pure water for 14 days. The experiments revealed weight losses of 0.02% and 0.05% for the crystalline and amorphous pyrochlore samples, respectively. The results of this study also indicated that the release rates of Cm and the radioactive daughter product ^{240}Pu increased by factors of 17 and 49, respectively, as a consequence of amorphization. It is instructive to compare the results of actinide doping experiments with the analogous situation wherein samples are irradiated using heavy ions and then subjected to dissolution tests. The irradiation of bulk pyrochlore using 2 MeV Au ions has been shown to produce an amorphous layer to depths of approximately 300–400 nm (Begg *et al.* 2001). Subsequent dissolution tests on crystalline and amorphous samples performed at 90 °C in a solution of nitric acid at pH = 2 gave different results, depending on the A-site cation in a series of $A_2Ti_2O_7$ pyrochlores with A = Y, Lu, and Gd. The process of amorphization in these samples caused the release rates of Y, Lu, and Gd to increase by factors of 0, 3–5, and 10–15, respectively. Stewart *et al.* (2003) recently reported similar results for a Ce-doped LLNL-type pyrochlore waste form irradiated with heavy ions. Dissolution of this material at 90 °C in a solution with pH = 1.75 suggested that the irradiation caused an increase in the release rates of Ca, Gd, and Ti by a factor of about 2–12 over those of the unirradiated sample. The results of both studies indicate that the elemental release rates of Ca and REEs are generally 1–2 orders of magnitude higher than Ti. As noted above, this may be due to precipitation of Ti-rich secondary phases on the surface of the sample.

Significant new results are now available (Icenhower *et al.* 2003) for synthetic pyrochlore samples with compositions corresponding to the LLNL Baseline Formulation with Ce or Pu–U, single-phase pyrochlore with Ce or Pu–U, and single-phase $Gd_2Ti_2O_7$ for comparison. The baseline and single phase Pu–U pyrochlores were fabricated with ^{238}Pu or ^{239}Pu in order to compare samples with high and low alpha-decay dose under identical conditions. The experiments were designed for single-pass flow through conditions allowing for a range of flow rate to surface area ratios, while at the same time minimizing experimental problems (e.g., effect of F from teflon, effect of atmospheric CO_2 on pH, and effect of radiolysis at low flow rates). Results for solutions buffered at pH = 2 and temperatures of 85–90 °C reveal that a steady-state, forward reaction rate can be determined for high values of the flow rate to surface area ratio. Under these conditions, Icenhower *et al.* (2003) report release rates of 1.3×10^{-3} g/m^2/d for the LLNL Baseline pyrochlore formulations and 2×10^{-4} g/m^2/d for the single-phase pyrochlores. However, the most important result of this work is that the dissolution rates of the crystalline and X-ray amorphous (^{238}Pu-doped) samples are the same, within the experimental errors.

Zirconolite ceramics and natural samples

Prior to 1988, dissolution studies had only been reported on natural samples and the results were complicated by the presence of inclusions (Ringwood *et al.* 1988). Nevertheless, the release rate of Ca from fully amorphous zirconolite from Sri Lanka, averaged over temperatures of 95 and 200 °C, appeared to decrease from about 10^{-1} g/m^2/d to 3×10^{-3} g/m^2/d after about 2 weeks. McGlinn *et al.* (1995) studied the pH dependence of single-phase zirconolite in pure flowing water at 90 °C. Results showed that after 43 days the release rates for Ca decrease with increasing pH for all samples, although there is a lot of scatter, especially where the data are close to the detection limit. Over the duration of the experiments,

the Ca rate of release dropped from about 10^{-2} to 10^{-3} g/m^2/d. Preferential release of Ca over Ti (by a factor of 10–450) occurred in all samples over the entire pH range. However, SEM work failed to show conclusive evidence for alteration products on the surface of the zirconolite. It is worth noting here that the Ca release rate of the amorphous natural zirconolite, extrapolated to 43 days, is approximately 2×10^{-3} g/m^2/d, suggesting that the alpha-decay induced amorphization has little influence on the long-term dissolution rate.

We have included here, for comparison, the results of a study of zirconolite-rich Synroc nominally composed of 80 wt% Ce- or Pu-doped zirconolite plus 10 wt% hollandite and 10 wt% rutile (Hart *et al.* 1998). Inclusion of this study in this section is significant because the two additional phases are both highly durable in their own right and the experiments were conducted at two different temperatures (90 and 200 °C) and in three different aqueous solutions (pure water, silicate, and brine). The authors found no major differences in the release rates of Ca, Ce, Hf, Ti, Zr, Pu, and Gd apart from those for Ce and Ti, which appeared to be somewhat higher in the brine. On average, for all elements, the increase in temperature caused the release rates to increase by a factor of approximately seven. Release rates were generally below 10^{-2} g/m^2/d for Ca, 10^{-3} g/m^2/d for Ce and Gd, and 10^{-4} g/m^2/d for Ti, Zr, Hf, and Pu (except for the brine at 200 °C, which gave a Ti release rate of 2×10^{-3} g/m^2/d). Hart *et al.* (2000) also determined the release rate of Pu in an LLNL-type zirconolite ceramic. After nearly one year in pure water at 90 °C the release rate of Pu decreased from 2×10^{-3} g/m^2/d to less than 10^{-5} g/m^2/d (Fig. 7).

The dissolution kinetics of zirconolite have now been determined as a function of pH using pure water in single-pass flow through tests at temperatures of 75 °C and lower (Roberts *et al.* 2000; Zhang *et al.* 2001*b*). These authors have independently studied a Ce-, Gd-, and Hf-doped zirconolite containing about 16 wt% UO_2 and the results of the two studies are similar. Release rates determined by Zhang *et al.* (2001*b*) indicate that Ti and U are released from zirconolite at about the same rate after about 20 days following an initial period where U is released at a somewhat faster rate than Ti. The limiting rate constants, K, are equivalent to U release rates of 6.4×10^{-7} to 1.3×10^{-5} g/m^2/d for zirconolite over the entire pH range of 2–12 and temperature range of 25–75 °C. The dissolution rate of zirconolite is characterized by a shallow V-shaped pattern with a minimum near pH = 8, similar to the results obtained for pyrochlore (Fig. 8).

Malmström and coworkers (Malmström *et al.* 1999, 2000; Malmström 2000) have investigated the performance of several zirconolite compositions under hydrothermal conditions (150–700 °C, 50–200 MPa) in fluids containing different concentrations of HCl, NaOH, H_3PO_4, silicate, or carbonate, in addition to pure water. Starting materials consisted of $Ca_{0.99}Zr_{1.07}Ti_{1.94}O_7$ and $Ca_{0.8}U_{0.2}ZrTi_{1.6}Al_{0.4}O_7$ with 1–3 wt% excess $CaZrTi_2O_7$, and single-phase samples of $Ca_{0.8}Nd_{0.2}ZrTi_{1.8}Al_{0.2}O_7$, $Ca_{0.85}Ce_{0.1}Gd_{0.1}Zr_{0.85}Hf_{0.1}Ti_{1.9}Al_{0.1}O_7$, and $Ca_{0.85}U_{0.1}Gd_{0.1}Zr_{0.85}Hf_{0.1}Ti_{1.8}Al_{0.2}O_7$. The results of these experiments demonstrate that zirconolite is most highly reactive in the NaOH-bearing fluids, but temperatures in excess of 500 °C are required to produce a continuous alteration layer consisting of perovskite + calzirtite at 50 MPa or perovskite + baddeleyite at 200 MPa. In the case of HCl, similar temperatures are required to produce an alteration layer consisting of rutile and anatase. Somewhat surprisingly, SEM observations revealed that the silicate and carbonate fluids had no visible effect on the zirconolite surface after experimental runs at 550 °C and 50 MPa. Only limited reaction was observed in pure water or H_3PO_4 fluids at the same temperature and pressure, with rutile and monazite appearing as products on the surface.

Brannerite ceramics

Vance *et al.* (2000) presented some preliminary results on the release of U from brannerite in flowing solutions buffered to three different pH values at 70 °C. After 60 days of testing, the U release rates were approximately 8×10^{-3}, 2×10^{-3}, and 10^{-4} g/m^2/d for solutions with pH = 2.1, 9.8, and 7.9, respectively. In addition to basic dissolution tests, many of these laboratory experiments were specifically designed to shed light on the kinetics and mechanisms of brannerite alteration. The aforementioned results have been extended to additional pH values and temperatures by Zhang *et al.* (2001*b*). For temperatures of 20–50 °C and pH values in the range of 2–12, these authors report limiting rate constants for U equivalent to elemental release rates of about 2×10^{-3} to 2×10^{-6} g/m^2/d. The lowest rate was obtained at 20 °C and pH = 5.6. However, the pH dependence was examined in detail at 70 °C and the results show a shallow V-shaped pattern similar to that of pyrochlore and zirconolite, although the release rates of U from these two phases are

1–2 orders of magnitude less than that of brannerite (Fig. 8).

In particular, Zhang *et al.* (2003) investigated the dissolution of brannerite as a function of pH, phthalate, and bicarbonate concentration in aqueous fluids at low temperature. Their results show that the initial uranium release rate is weakly dependent on phthalate concentration with the reaction order of 0.19 and then approaches a constant value after about one hour. There is no obvious rate dependence of titanium on phthalate concentration and the uranium release rate is 2–3 orders of magnitude greater than titanium. Furthermore, experimental results show that the phthalate ion increases titanium solubility. In bicarbonate solutions, however, the uranium release rate is strongly dependent on bicarbonate concentration with the initial reaction order of ~0.5, increasing to ~0.7 after 7 days. Therefore, the concentration of bicarbonate enhances the dissolution of brannerite under alkaline conditions (cf. Szymański and Scott, 1982). In the same experiments, the release of titanium is not dependent upon bicarbonate concentration, either in release rate or equilibrium concentration (~3 ppb), indicating that unlike phthalate, bicarbonate does not interact strongly with titanium, either on the solid surface or in solution.

Further experiments by Zhang *et al.* (2003) using ion beam thinned sections (for subsequent TEM examination) show that for a pH 2 solution, an apparent preferential release of uranium occurs (Fig. 9). Results from TEM show that the IBT specimen tested in pH 2 solution at 90 °C for four weeks has large areas of unaltered brannerite as well as a relatively small amount of secondary phase. The primary rutile grains appear to have been partially etched. Energy dispersive X-ray (EDX) spectroscopy indicates that the secondary phase is TiO_2 with differing amounts of uranium and trace amounts of other elements. Selected area electron diffraction confirms that the secondary phase is polycrystalline, probably anatase and/or brookite. In the case of pH 11 solution, the less linear and lower release of uranium than titanium suggests that some dissolved uranium may absorb back onto the secondary phase or even the sample itself. Overall, the release rates of U and Ti from the IBT specimen in pH 11 solution are nearly the same. The IBT specimen exposed to pH 11 solution at 90 °C for four weeks shows large areas of a fibrous secondary phase associated with the original brannerite. Selected area electron diffraction indicates that the secondary phase is amorphous. Energy dispersive X-ray spectroscopy shows that the Ti-rich secondary phase contains varying amounts of uranium and trace amounts of other elements. Also, XPS analyses indicate the existence of oxidized U^{5+} and U^{6+} species on specimens both before and after the dissolution tests, and U^{6+} was the dominant component on the specimen tested in the pH 11 solution.

Hollandite ceramics

Experimental studies of the polyphase ceramics noted above demonstrate that hollandite is one of the most durable titanate phases in aqueous solutions. Pham *et al.* (1994) carried out experimental work on synthetic Ba–hollandite doped with Cs and containing Al on the B-site for charge balance. These authors suggested that, following the initial release of Cs and Ba from reactive surface sites the first few monolayers of the structure rapidly dissolved due to the release of Al and consequent precipitation of Al-OH species, driving solution pH to lower values. However, the alteration process was mediated via the formation of a continuous Al- and Ti-rich surface layer. Further evidence for selective removal of Ba and enrichment of Al and Ti on the surface of hollandite tested at 250–300 °C was presented by Myhra *et al.* (1988*b*). These conclusions were largely based on the different release rates of Ba (10^{-1} g/m^2/d), Al (7×10^{-3} g/m^2/d), and Ti ($<8 \times 10^{-4}$ g/m^2/d) after 14 days of dissolution testing, combined with XPS analyses of the altered surfaces.

Recent work by Carter *et al.* (2002) on the alteration of hollandite samples in pure water at 90 °C and 150 °C demonstrates that the release rates of Ba and Cs are nearly identical. In these same experiments, Al and Ti are below detection limits at 90 °C and only Al is detected at 150 °C, but only by a factor of 2–3 above the detection limit. These authors also examined the pH dependence of the release rates at 90 °C, finding that the release of Ba decreases linearly (Fig. 8) from about 2×10^{-3} g/m^2/d at pH = 2.5 to 4×10^{-4} g/m^2/d at pH = 12.9. SEM work revealed the presence of nodular secondary phases on the surface of the hollandite at both temperatures. This was confirmed by XTEM work on cross-sections of the material, which identified both Ti-rich and Al-rich nodules in a ratio of about ten to one, respectively. Furthermore, XPS analysis of the hollandite surface after testing at 150 °C for 7 days showed an increase in the Al/Ti ratio from 0.26 to 0.47, consistent with the presence of an Al-rich layer approximately 0.5 nm thick. XPS results also show a decrease in the Ba/Ti ratio from 0.095 to 0.072 and this is equivalent to removal of about 25% of the Ba within 5 nm of the surface.

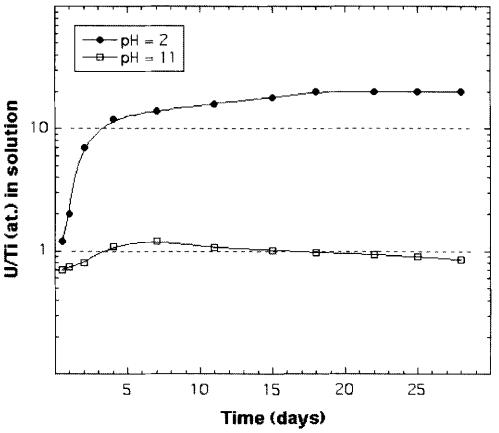

Fig. 9. Graph showing the change in U/Ti atomic ratio in the fluid (normalized to the stoichiometry of the starting material) after dissolution of synthetic brannerite acidic and basic fluids (after Zhang *et al.* 2003). The experiment at pH = 2 reveals a strong preferential release of U, reaching a steady-state normalized U/Ti atomic ratio of about 20 after several weeks.

The effects described above by Carter *et al.* (2002) are further illustrated in Fig. 10. Here we plot variations in the concentrations of Al_2O_3, Fe_2O_3, Cs_2O, and BaO determined by AEM from replicas of hollandite removed from the surface of Synroc-C tested at 150 °C in pure water for up to 532 days. These analyses indicate that there is an accumulation of Al–Fe–O–H material on the surface of hollandite up to about 150–200 days of testing. If the hollandite grains have thicknesses of 25–75 nm, typical values for AEM analysis, then the increases in Al_2O_3 and Fe_2O_3 content correspond to a surface layer thickness of approximately 1–3 nm. The AEM analyses also reveal significant decreases in the Cs_2O and BaO content, the magnitude of which cannot be fully explained by the Al–Fe–O–H layer. Therefore, it can be postulated that the tunnel cations have been released to a depth of 8–16 nm depending upon the actual hollandite crystal thickness used for the AEM analyses. The overall alteration mechanism is illustrated in Figure 11 and is generally consistent with the observations of Carter *et al.* (2002) and the hollandite alteration depth estimated from elemental release data.

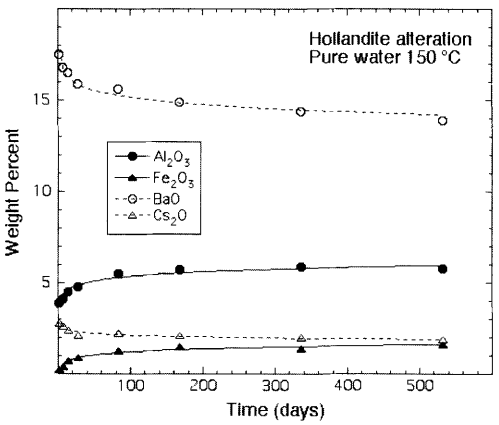

Fig. 10. Change in composition of thin hollandite grains, lifted from the surface of Synroc-C, as determined by AEM after leaching in pure water at 150 °C for up to 532 days. The measured concentrations of BaO and Cs_2O decrease whereas the concentrations of Al_2O_3 and Fe_2O_3 increase with time. There is also a slight increase in the TiO_2 concentration out to 532 days (not shown). See text and Fig. 11 for further discussion and an illustration of hollandite alteration.

Perovskite ceramics and natural samples

Nesbitt *et al.* (1981) performed a detailed analysis of the thermodynamic and kinetic stability of perovskite. Thermodynamic calculations and data for natural groundwaters and hydrothermal

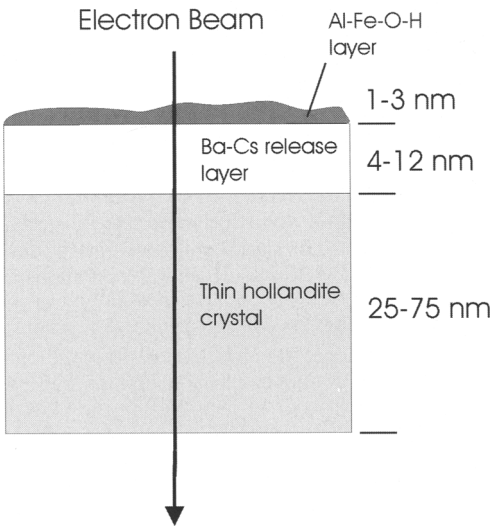

Fig. 11. Schematic drawing of the alteration of hollandite, as deduced from material recovered on TEM replicas (see Fig. 10). The model assumes a thickness of 50–100 nm for the hollandite grains and a uniform thickness of Al–Fe–O–H material built up on the surface during the alteration process. The decrease in the measured concentration of Ba, for example, cannot exceed that required by the surface layer alone and requires additional Ba release to a depth of approximately 8–16 nm depending on the actual grain thickness.

fluids (up to 300 °C) revealed that perovskite is unstable with respect to titanite, titanite + quartz, quartz, rutile, or rutile + calcite. The groundwaters used in this study represented a range of compositions emanating from dunites, peridotites, serpentinites, rhyolites, granites, and limestones. This work included measurements of the dissolution rates of two natural perovskites and synthetic $SrTiO_3$ and $BaTiO_3$ samples in pure water at 25–300 °C. Results of the experimental work gave elemental release rates in the range of 5×10^{-2} to 8×10^{-1} g/m^2/d for Ca, 4×10^{-2} to 3×10^{-1} g/m^2/d for Sr, and 3×10^{-2} to 4×10^{-1} g/m^2/d for Ba. The Ca release rates were obtained from a single crystal from Magnet Cove, Arkansas. Using a powdered sample of perovskite from Australia, lower release rates of 10^{-3} to 10^{-2} g/m^2/d for Ca have been reported. Kamizono *et al.* (1991) have also examined the behaviour of $CaZrO_3$ in acidic (HCl, pH = 1) and near neutral (deionized water, pH = 5.6) solutions at 90 °C. The release rates of Ca and Zr were determined to be 10^{-3} g/m^2/d and 2×10^{-4} g/m^2/d, respectively, in the experiment with pH = 1. Release rates were about two orders of magnitude lower in the experiment using deionized water (see figs 1 and 2 in Kamizono *et al.* 1991). As noted above, the perovskite contained small amounts of Ce, Nd, and Sr as simulated waste elements. These elements had unusually high release rates of about 10^{-1} g/m^2/d.

Surface analytical studies of synthetic perovskite after experiments conducted at 150–250 °C in silica saturated aqueous fluids were reported by Myhra *et al.* (1987). These authors, using a combination of AES, SEM-EDX, and XPS techniques, identified the presence of a surface reaction layer ranging in thickness from a few monolayers to several hundred nanometers, depending on the experimental conditions. In spite of the presence of SiO_2 and CO_2 in solution (the system was open to the atmosphere), the alteration layer was composed mainly of crystalline TiO_2, a thin siliceous layer, and possible calcium carbonate or hydroxide species. Following this work, Myhra *et al.* (1988*b*) reported additional results for $CaTiO_3$ and $BaTiO_3$ tested at 300 °C in pure water. They determined release rates after 14 days of 10^{-2} g/m^2/d for Ca and 3×10^{-2} g/m^2/d for Ba from the two samples, respectively. Surface analytical work showed that Ca and Ba were depleted to a depth of about 200 nm and that oxygen was enriched near the surface, consistent with the release of Ca and Ba to solution and the formation of a crystalline TiO_2 layer.

Pham and co-workers have performed similar experiments at temperatures of 20–100 °C. These authors showed that near surface decreases in the Ca/Ti ratio determined by XPS are accompanied by the formation of an amorphous Ti-rich layer up to 10 nm thick, as observed by TEM (Pham *et al.* 1989; Turner *et al.* 1989). The authors proposed a base catalysed hydrolysis and ion exchange model to account for their observations, whereby surface Ca^{2+} is released to solution via exchange with H^+ and Ti–O–Ti surface species are converted to Ti–OH species via reaction with OH^- and H_2O. The overall reaction can be written as follows (Pham *et al.* 1989):

$$CaTiO_3 + (6 - x)H^+ = Ca^{2+} + Ti(OH)_x^{(4-x)+} + (3 - x)H_2O$$

This reaction indicates that the aqueous Ca^{2+}/H^+ ratio and the presence of Ti–OH surface species control the dissolution of perovskite. The presence of the amorphous Ti–OH surface film at low temperatures may be due to kinetic factors, as crystalline TiO_2 phases are thermodynamically favoured at low temperatures (Pham *et al.* 1989). McGlinn *et al.* (1995) investigated the pH dependence of the release of Ca from two perovskite samples: end-member $CaTiO_3$ and $Ca_{0.78}Sr_{0.04}Nd_{0.18}Ti_{0.82}Al_{0.18}O_3$. Results of this study, performed at 90 °C with pH ranging from 2.1 to 12.9, demonstrated that the Ca release rates generally decrease with increasing pH. After 43 days of testing, the Ca release rate for the end-member perovskite decreased from just below 10^{-1} g/m^2/d at pH = 2.1 to 2×10^{-3} g/m^2/d at pH = 12.9. Similar results were obtained for the doped perovskite, in which the Ca release rate decreased from 4×10^{-2} g/m^2/d at pH = 2.1 to less than 2×10^{-3} g/m^2/d at pH = 12.9. These results are summarized in Figure 8. In SEM imaging the development of 'agglomerated, submicron, titanaceous particles' are clearly shown on the perovskite surface after testing under acidic conditions.

Discussion and conclusions

Using the criteria listed in the introduction, we now provide a brief summary of the performance of these materials. With reference to criterion number 5, physical properties, we restrict out discussion here to the effects of radiation damage on the crystalline structure. For materials destined for geological disposal, the long-term performance in natural systems over long periods of time (e.g., 10^3 to 10^6 years) is of critical concern. Therefore, we believe that it is necessary to consider one more criterion: (6) natural samples exist and allow for an assessment of the

long-term behaviour. Using these criteria as a guide, we illustrate below some of the advantages and disadvantages of these waste form phases.

Starting from the requirement of aqueous durability, the data summarized in this paper clearly demonstrate that perovskite is the least durable phase present in the polyphase waste forms such as Synroc-C. As described above, the low-temperature alteration of perovskite to anatase and other phases in natural systems is well known. These results are consistent with the available thermodynamic data and are generally corroborated by laboratory experiments on single-phase and polyphase samples. Most of these experiments have been executed at temperatures of 70–150 °C in pure water, with fewer studies concerning the performance in sodium chloride, bicarbonate, and silicate solutions, or at temperatures above and below the stated range. Characterization studies have shown that perovskite readily reacts with aqueous fluids to form an amorphous Ti–O–H film at temperatures below about 100 °C or crystalline TiO_2 polymorphs at higher temperatures. Therefore, from a natural systems and experimental viewpoint, perovskite is not the best host phase for either ACTs or Sr in waste forms destined for a geological repository. Note, however, that these comments largely apply to ACT-poor perovskite compositions in the system $CaTiO_3$–$SrTiO_3$–$REETiO_3$–$REEAlO_3$ with $CaTiO_3$ as the dominant component.

The kinetics and mechanisms of brannerite alteration in aqueous fluids are now reasonably well established through experiments covering a range of temperature, fluid composition, and pH. Although generally highly resistant to total dissolution due to the low solubility of the TiO_2 component, brannerite is susceptible to chemical alteration by ion exchange and recrystallization processes. However, the overall influence of this phase on waste form performance, at least in terms of U release, should be minimal as long as the volume proportion is kept low (e.g., below approximately 10 vol%). Furthermore, recent experimental work has shown that end-member brannerite, UTi_2O_6, is energetically stable with respect to the oxide assemblage $UO_2 + 2TiO_2$, with $\Delta H^0_{f\text{-}ox} = -7.7$ kJ/mol at 25 °C (Helean *et al.* 2003). End-member $PuTi_2O_6$ is metastable with respect to the oxides $PuO_2 + TiO_2$; however, Helean *et al.* (2003) estimate that inclusion of up to 30% brannerite of composition $U_{0.8}Pu_{0.2}Ti_2O_6$ will not significantly alter the thermodynamic stability of the waste form.

Pyrochlore and zirconolite have excellent release rates with minimal variation as a function of pH, they are highly flexible in terms of their ability to incorporate impurities, they are well established with regard to processing, and they can accommodate substantial waste loadings. Both the aqueous performance and radiation effects determined experimentally are confirmed through studies of natural samples. The general chemistry and alteration mechanisms of natural pyrochlores in the system $NaCaNb_2O_6F$–$NaCaTa_2O_6F$–$Ca_2Nb_2O_7$–$Ca_2Ta_2O_7$–$REE_2Ti_2O_7$–$CaUTi_2O_7$ are well documented. Alteration processes are dominated by ion exchange effects, but these are largely restricted to the Nb–Ta end-members due to the nature of the structure and bonding (Lumpkin 2001, p. 160). Some evidence for dissolution and reprecipitation of pyrochlore has been presented, but only in the most extreme geological environments. In fact, the world's largest Nb ore deposits are formed through the dissolution of the host rocks and concentration of pyrochlore in overlying laterite horizons. Studies of natural samples suggest that zirconolite is even more durable that pyrochlore, consistent with experimental evidence and the nature of the crystal structure. Although titanate pyrochlore and zirconolite are rendered amorphous by alpha-decay processes, the *total volume expansion is low* (5–6%) and the *effect of amorphization on aqueous durability is negligible* (e.g., Icenhower *et al.* 2003). Of the two phases, the performance of zirconolite appears to be somewhat better than that of pyrochlore in both the experimental and natural systems. Additionally, zirconolite is one of the few host phases subjected to experimentation at elevated temperature and pressure and in a range of fluid compositions, and the results indicate that this mineral is highly resistant to aqueous attack up to about 250–400 °C in a range of fluid compositions. The titanate pyrochlore and zirconolite-rich waste forms both appear to be thermodynamically stable relative to the oxides or to assemblages containing perovskite + oxides (e.g., Putnam *et al.* 1999; Helean *et al.* 2002).

Finally, hollandite is the only non-actinide host phase considered here, and is the only Cs host phase that has been extensively studied. Results summarized herein indicate that hollandite has excellent aqueous durability, crystal chemical flexibility, well-known processing parameters, and more than adequate waste loadings. Although natural analogues exist for hollandite, they have not been examined in the context of nuclear waste disposal, thus we have no details on the long-term behaviour of this important Cs host phase.

We thank J. P. Icenhower and T. Advocat for constructive reviews of this manuscript. Further credit must be given to

M. G. Blackford, B. C. Chakoumakos, M. Colella, R. A. Day, R. C. Ewing, K. P. Hart, A. Jostsons, A. N. Mariano, E. R. Vance, and F. Wall, among others, for their significant contributions to this work. Natural samples provided by the American Museum of Natural History, Australian Museum, Australian National University, ETH Zürich, Harvard University, The Natural History Museum have formed much of the basis of this work. We acknowledge funding support over many years from the Australian Nuclear Science and Technology Organisation the United States Department of Energy. The Cambridge Centre for Ceramic Immobilisation is supported by British Nuclear Fuels Limited and the Cambridge-MIT Institute.

References

BALL, C. J., BUYKX, W. J. *et al.* 1989. Titanate ceramics for the stabilization of partially reprocessed nuclear fuel elements. *Journal of the American Ceramic Society*, **72**, 404–414.

BANFIELD, J. F. & VEBLEN, D. R. 1992. Conversion of perovskite to anatase and TiO_2 (B): A TEM study and the use of fundamental building blocks for understanding relationships among the TiO_2 minerals. *American Mineralogist*, **77**, 545–557.

BART, F., LETURCQ, G. & RABILLER, H. 2003. Iron-substituted barium hollandite ceramics for cesium immobilization. *105th American Ceramic Society Symposium Proceedings*, Nashville, TN, USA, 27 April–2 May.

BEGG, B. D., HESS, N. J., WEBER, W. J., DEVANATHAN, R., ICENHOWER, J. P., THEVUTHASAN, S. & MCGRAIL, B. P. 2001. Heavy-ion irradiation effects on structures and acid dissolution of pyrochlores. *Journal of Nuclear Materials*, **288**, 208–216.

BELLATRECCIA, F., DELLA VENTURA, G., CAPRILLI, E., WILLIAMS, C. T. & PARODI, G. C. 1999. Crystal-chemistry of zirconolite and calzirtite from Jacupirange, São Paulo (Brazil). *Mineralogical Magazine*, **63**, 649–660.

BELLATRECCIA, F., DELLA VENTURA, G., WILLIAMS, C. T., LUMPKIN, G. R., SMITH, K. L. & COLELLA, M. 2002. Non-metamict zirconolite polytypes from the feldspathoid-bearing alkali-syenitic ejecta of the Vico volcanic Complex (Latium, Italy). *European Journal of Mineralogy*, **14**, 809–820.

BULAKH, A. G., NESTEROV, A. R., WILLIAMS, C. T. & ANISIMOV, I. S. 1998. Zirkelite from the Sebl'yavr carbonatite complex, Kola peninsula, Russia: and x-ray and electron microprobe study of a partially metamict mineral. *Mineralogical Magazine*, **62**, 837–846.

CARTER, M. L., VANCE, E. R., MITCHELL, D. R. G., HANNA, J. V., ZHANG, Z. & LOI, E. 2002. Fabrication, characterisation, and leach testing of hollandite, $(Ba,Cs)(Al,Ti)_2Ti_6O_{16}$. *Journal of Materials Research*, **17**, 2578–2589.

CHAKHMOURADIAN, A. R. & MITCHELL, R. H. 1998. Lueshite, pyrochlore and monazite-(Ce) from apatite–dolomite carbonatite, Lesnaya Varaka complex, Kola Peninsula, Russia. *Mineralogical Magazine*, **62**, 769–782.

CHAKHMOURADIAN, A. R., MITCHELL, R. H., PANKOV, A. V. & CHUKANOV, N. V. 1999. Loparite and 'metaloparite' from the Burpala alkaline comples, Baikal Alkaline Province (Russia). *Mineralogical Magazine*, **63**, 519–534.

CHAKOUMAKOS, B. C. 1984. Systematics of the pyrochlore structure type, ideal $A_2B_2X_6Y$. *Journal of Solid State Chemistry*, **53**, 120–129.

CHEARY, R. W. 1987. A structural analysis of potassium, rubidium and caesium substitution in barium hollandite. *Acta Crystallographica*, **B43**, 28–34.

CHEARY, R. W. 1988. The immobilisation of cesium in synroc. *Materials Science Forum*, **27/28**, 397–406.

CROVISIER, J. L., ADVOCAT, T. & DUSSOSSOY, J. L. 2004. Relevance of analogues for long-term prediction. *In*: GIERÉ, R. & STILLE, P. (eds). *Energy, Waste, and the Environment: a Geochemical Perspective*. Geological Society, London, Special Publications, **236**, 113–121.

DONALD, I. W., METCALFE, B. L. & TAYLOR, R. N. J. 1997. The immobilisation of high level radioactive wastes using ceramics and glasses. *Journal of Materials Science*, **32**, 5851–5887.

EWING, R. C., WEBER, W. J. & CLINARD, F. W., JR. 1995. Radiation effects in nuclear waste forms for high-level radioactive waste. *Progress in Nuclear Energy*, **29**, 63–127.

EWING, R. C., HAAKER, R. F., HEADLEY, T. J. & HLAVA, P. F. 1982. Zirconolites from Sri Lanka, South Africa and Brazil. *In*: TOPP, S. V. (ed) *Scientific Basis for Nuclear Waste Management* V. Elsevier, New York, 249–256.

FIELDING, P. E. & WHITE, T. J. 1987. Crystal chemical incorporation of high level waste species in aluminotitanate-based ceramics: valence, location, radiation damage, and hydrothermal durability. *Journal of Materials Research*, **2**, 387–414.

FILLET, C., ADVOCAT, T. *et al.* 2002. Des matrices sur mesure pour les radionucléides à vie longue. Les researches pour la gestion des déchets nucléairs ISSN 0298-6248. *CLEFS CEA*, **46**, 64–67.

FILLET, C., ADVOCAT, T., BART, F., LETURCQ, G. & RABILLER, H. 2004. Titanate ceramics for separated long-lived radionuclides. Compte rendu de l'Académie des Sciences, in press.

GIERÉ, R. & WILLIAMS, C. T. 1992. REE-bearing minerals in a Ti-rich vein from the Adamello contact aureole (Italy). *Contributions to Mineralogy and Petrology*, **112**, 83–100.

GIERÉ, R., WILLIAMS, C. T. & LUMPKIN, G. R. 1998. Chemical characteristics of natural zirconolite. *Schweiz. Mineral. Petrogr. Mitt.*, **78**, 433–459.

GIERÉ, R., GUGGENHEIM, R. *et al.* 1994. Retention of actinides during alteration of aperiodic zirconolite. *ICEM 13 Paris*, 1269–1270.

GIERÉ, R., SWOPE, R. J., BUCK, E. C., GUGGENHEIM, R., MATHYS, D. & REUSSER, E. 2000. Growth and alteration of uranium-rich microlite. *In*: SMITH, R. W. & SHOESMITH, D. W. (eds) Scientific Basis for Nuclear Waste Management XXIII. *Materials Research Society Symposium Proceedings*, **608**, 519–524.

GIERÉ, R., BUCK, E. C., GUGGENHEIM, R., MATHYS, D., REUSSER, E. & MARQUES, J. 2001. Alteration of

Uranium-rich Microlite. *In*: HART, K. P. & LUMPKIN, G. R. (eds) Scientific Basis for Nuclear Waste Management XXIV. *Materials Research Society Symposium Proceedings*, **663**, 935–944.

HARKER, A. B. 1988. Tailored ceramics. *In*: LUTZE, W. & EWING, R. C. (eds) *Radioactive Waste Forms for the Future*. North-Holland, Amsterdam, 335–392.

HART, K. P., GLASSLEY, W. E. & MCGLINN, P. J. 1992. Solubility control of actinide elements leached from Synroc in pH-buffered solutions. *Radiochimica Acta*, **58/59**, 33–35.

HART, K. P., LUMPKIN, G. R., GIERÉ, R., WILLIAMS, C. T., MCGLINN, P. J. & PAYNE, T. E. 1996. Naturally occurring zirconolites – analogues for the long-term encapsulation of actinides in Synroc. *Radiochimica Acta*, **74**, 309–312.

HART, K. P., VANCE, E. R. *et al.* 1998. Leaching behaviour of zirconolite-rich synroc used to immmobilise 'high-fired' plutonium oxide. *In*: MCKINLEY, I. G. & MCCOMBIE, C. (eds) Scientific Basis for Nuclear Waste Management XXI. *Materials Research Society Symposium Proceedings*, **506**, 161–168.

HART, K. P., ZHANG, Y. *et al.* 2000. Aqueous durability of titanate ceramics designed to immobilise excess Pu. *In*: SMITH, R. W. & SHOESMITH, D. W. (eds) Scientific Basis for Nuclear Waste Management XXIII. *Materials Research Society Symposium Proceedings*, **608**, 353–358.

HELEAN, K. B., NAVROTSKY, A. *et al.* 2002. Enthalpies of formation of Ce–pyrochlore, $Ca_{0.93}Ce_{1.00}Ti_{2.035}O_{7.00}$, U–pyrochlore, $Ca_{1.46}U^{4+}_{0.23}U^{6+}_{0.46}Ti_{1.85}O_{7.00}$ and Gd–pyrochlore, $Gd_2Ti_2O_7$: three materials relevant to the proposed waste form for excess weapons plutonium. *Journal of Nuclear Materials*, **303**, 226–239.

HELEAN, K. B., NAVROTSKY, A. *et al.* 2003. Enthalpies of formation of U–, Th–, Ce–brannerite: implications for plutonium immobilisation. *Journal of Nuclear Materials*, **320**, 231–244.

ICENHOWER, J. P., MCGRAIL, B. P., SCHAEF, H. T. & RODRIQUEZ, E. A. 2000. Dissolution kinetics of titanium pyrochlore ceramics at 90 °C by single-pass flow-through experiments. *In*: SMITH, R. W. & SHOESMITH, D. W. (eds) Scientific Basis for Nuclear Waste Management XXIII. *Materials Research Society Symposium Proceedings*, **608**, 373–378.

ICENHOWER, J. P., STRACHAN, D. M., LINDBERG, M. M., RODRIQUEZ, E. A. & STEELE, J. L. 2003. *Dissolution Kinetics of Titanate-Based Ceramic Waste Forms: Results from Single-Pass Flow Tests on Radiation Damaged Specimens*. Pacific Northwest National Laboratory, Report No. PNNL-14252.

KAMIZONO, H., HAYAKAWA, I. & MURAOKA, S. 1991. Durability of zirconium-containing ceramic waste forms in water. *Journal of the American Ceramic Society*, **74**, 863–864.

KASTRISSIOS, T., STEPHENSON, M., TURNER, P. S. & WHITE, T. J. 1987. Hydrothermal dissolution of perovskite: implications for synroc formulation. *Journal of the American Ceramic Society*, **70**, C-144–C-146.

KESSON, S. E. 1983. The immobilisation of cesium in synroc hollandite. *Radioactive Waste Management and the Nuclear Fuel Cycle*, **4**, 53–72.

KESSON, S. E. & WHITE, T. J. 1986*a*. $[Ba_xCs_y][(Ti,Al)^{3+}_{2x+y}Ti^{4+}_{8-2x-y}]O_{16}$ Synroc-type hollandites I. Phase chemistry. *Proceedings of the Royal Society of London*, **A 405**, 73–101.

KESSON, S. E. & WHITE, T. J. 1986*b*. $[Ba_xCs_y][(Ti,Al)^{3+}_{2x+y}Ti^{4+}_{8-2x-y}]O_{16}$ Synroc-type hollandites II. Structural chemistry. *Proceedings of the Royal Society of London*, **A 408**, 295–319.

KOGARKO, L. N., WILLIAMS, C. T. & WOOLLEY, A. R. 2002. Chemical evolution of loparite through the layered, peralkaline Lovozero complex, Kola Peninsula, Russia. *Mineralogy and Petrology*, **74**, 1–24.

LETURCQ, G., ADVOCAT, T., HART, K., BERGER, G., LACOMBE, G. & BONNETIER, A. 2001. Solubility study of Ti,Zr-based ceramics designed to immobilize long-lived radionuclides. *American Mineralogist*, **86**, 871–880.

LUMPKIN, G. R. 1998. Rare-element mineralogy and internal evolution of the Rutherford #2 pegmatite, Amelia County, Virginia: a classic locality revisited. *Canadian Mineralogist*, **36**, 339–353.

LUMPKIN, G. R. 2001. Alpha-decay damage and aqueous durability of actinide host phases in natural systems. *Journal of Nuclear Materials*, **289**, 136–166.

LUMPKIN, G. R. & EWING, R. C. 1992. Geochemical alteration of pyrochlore group minerals: Microlite subgroup. *American Mineralogist*, **77**, 179–188.

LUMPKIN, G. R. & EWING, R. C. 1995. Geochemical alteration of pyrochlore group minerals: Pyrochlore subgroup. *American Mineralogist*, **80**, 732–743.

LUMPKIN, G. R. & EWING, R. C. 1996. Geochemical alteration of pyrochlore group minerals: Betafite subgroup. *American Mineralogist*, **81**, 1237–1248.

LUMPKIN, G. R. & MARIANO, A. N. 1996. Natural occurrence and stability of pyrochlore in carbonatites, related hydrothermal systems, and weathering environments. *In*: MURPHY, W. M. & KNECHT, D. A. (eds) Scientific Basis for Nuclear Waste Management XIX. *Materials Research Society Symposium Proceedings*, **412**, 831–838.

LUMPKIN, G. R., CHAKOUMAKOS, B. C. & EWING, R. C. 1986. Mineralogy and radiation effects of microlite from the Harding pegmatite, Taos County, New Mexico. *American Mineralogist*, **71**, 569–588.

LUMPKIN, G. R., SMITH, K. L. & BLACKFORD, M. G. 1991. Electron microscope study of Synroc before and after exposure to aqueous solutions. *Journal of Materials Research*, **6**, 2218–2233.

LUMPKIN, G. R., SMITH, K. L. & BLACKFORD, M. G. 1995. Development of secondary phases on synroc leached at 150 °C. *In*: MURAKAMI, T. & EWING, R. C. (eds) Scientific Basis for Nuclear Waste Management XVIII. *Materials Research Society Symposium Proceedings*, **353**, 855–862.

LUMPKIN, G. R., LEUNG, S. H. F. & COLELLA, M. 2000. Composition, geochemical alteration, and alpha-decay damage effects of natural brannerite. *In*: SMITH, R. W. & SHOESMITH, D. W. (eds) Scientific

Basis for Nuclear Waste Management XXIII. *Materials Research Society Symposium Proceedings*, **608**, 359–365.

LUMPKIN, G. R., HART, K. P., MCGLINN, P. J., PAYNE, T. E., GIERÉ, R. & WILLIAMS, C. T. 1994. Retention of actinides in natural pyrochlores and zirconolites. *Radiochimica Acta*, **66/67**, 469–474.

LUMPKIN, G. R., COLELLA, M., SMITH, K. L., MITCHELL, R. H. & LARSEN, A. O. 1998. Chemical composition, geochemical alteration, and radiation effects in natural perovskite. *In*: MCKINLEY, I. G. & MCCOMBIE, C. (eds) Scientific Basis for Nuclear Waste Management XXI. *Materials Research Society Symposium Proceedings*, **506**, 207–214.

LUMPKIN, G. R., DAY, R. A., MCGLINN, P. J., PAYNE, T. E., GIERÉ, R. & WILLIAMS, C. T. 1999. Investigation of the long-term performance of betafite and zirconolite hydrothermal veins from Adamello, Italy. *In*: WRONKIEWICZ, D. J. & LEE, J. H. (eds) Scientific Basis for Nuclear Waste Management XXII. *Materials Research Society Symposium Proceedings*, **556**, 793–800.

MALMSTRÖM, J. C. 2000. Zirconolite: experiments on the stability in hydrothermal fluids. *Beiträge zur Geologie der Schweiz, Geotechnische Serie*, **93**, 130 pp.

MALMSTRÖM, J. C., REUSSER, E., GIERÉ, R., LUMPKIN, G. R., DÜGGELIN, M., MATHYS, D. & GUGGENHEIM, R. 1999. Zirconolite corrosion in dilute acidic and basic fluids at 180–700 °C and 50 MPa. *In*: WRONKIEWICZ, D. J. & LEE, J. H. (eds) Scientific Basis for Nuclear Waste Management XXII. *Materials Research Society Symposium Proceedings*, **556**, 165–172.

MALMSTRÖM, J. C., REUSSER, E. *et al.* 2000. Formation of perovskite and calzirtite during zirconolite alteration. *In*: SMITH, R. W. & SHOESMITH, D. W. (eds) Scientific Basis for Nuclear Waste Management XXIII. *Materials Research Society Symposium Proceedings*, **608**, 475–480.

MARIANO, A. N. 1989. Economic geology of rare earth minerals. *In*: LIPIN, B. R. & MCKAY, G. A. (eds) Geochemistry and mineralogy of rare earth elements. *Reviews in Mineralogy*, **21**, 309–337.

MAZZI, F. & MUNNO, R. 1983. Calciobetafite (new mineral from the pyrochlore group) and related minerals from Campi Flegrei, Italy: crystal structure of polymignite and zirkelite: comparison with pyrochlore and zirconolite. *American Mineralogist*, **68**, 262–276.

MCGLINN, P. J., HART, K. P., LOI, E. H. & VANCE, E. R. 1995. pH Dependence of the aqueous dissolution rates of perovskite and zirconolite at 90 °C. *In*: MURAKAMI, T. & EWING, R. C. (eds) Scientific Basis for Nuclear Waste Management XVIII. *Materials Research Society Symposium Proceedings*, **353**, 847–854.

MITAMURA, H., MATSUMOTO, S. *et al.* 1992. Aging effects on curium-doped titanate ceramic containing sodium-bearing high-level nuclear waste. *Journal of the American Ceramic Society*, **75**, 392–400.

MITAMURA, H., MATSUMOTO, S. *et al.* 1994. α-Decay damage effects in curium-doped titanate ceramic containing sodium-free high-level nuclear waste. *Journal of the American Ceramic Society*, **77**, 2255–2264.

MITCHELL, R. H. 1996. Perovskites: a revised classification scheme for an important rare earth element host in alkaline rocks. *In*: JONES, A. P., WALL, F. & WILLIAMS, C. T. (eds) *Rare Earth Minerals, Chemistry, Origin and Ore Deposits*. Chapman and Hall, London, 41–76.

MITCHELL, R. H. & CHAKHMOURADIAN, A. R. 1998*a*. Th-rich loparite from the Khibina alkaline complex, Kola Peninsula: isomorphism and paragenesis. *Mineralogical Magazine*, **62**, 341–353.

MITCHELL, R. H. & CHAKHMOURADIAN, A. R. 1998*b*. Instability of perovskite in a CO_2-rich environment: examples from carbonatite and kimberlite. *Canadian Mineralogist*, **36**, 939–952.

MURAKAMI, T. 1985. Crystalline product on surface of synroc after long leaching. *Journal of Nuclear Materials*, **135**, 288–291.

MYHRA, S., WHITE, T. J., KESSON, S. E. & RIVIÉRE, J. C. 1988*a*. X-ray photoelectron spectroscopy for the direct identification of Ti valence in $[Ba_xCs_y][(Ti,Al)^{3+}_{2x+y}Ti^{4+}_{8-2x-y}]O_{16}$ hollandites. *American Mineralogist*, **73**, 161–167.

MYHRA, S., SMART, R. ST. C. & TURNER, P. S. 1988*b*. The surfaces of titanate minerals, ceramics and silicate glasses: surface analytical and electron microscope studies. *Scanning Microscopy*, **2**, 715–734.

MYHRA, S., DELOGU, P., GIORGI, R. & RIVIÉRE, J. C. 1988*c*. Scanning and high-resolution Auger analysis of zirconolite/perovskite surfaces following hydrothermal treatment. *Journal of Materials Science*, **23**, 1514–1520.

MYHRA, S., BISHOP, H. E., RIVIÉRE, J. C. & STEPHENSON, M. 1987. Hydrothermal dissolution of perovskite ($CaTiO_3$). *Journal of Materials Science*, **22**, 3217–3226.

NASRAOUI, M., BILAL, E. & GIBERT, R. 1999. Fresh and weathered pyrochlore studies by Fourier transform infrared spectroscopy coupled with thermal analysis. *Mineralogical Magazine*, **63**, 567–578.

NESBITT, H. W., BANCROFT, G. M., FYFE, W. S., KARKHANIS, S. N. & NISHIJIMA, A. 1981. Thermodynamic stability and kinetics of perovskite dissolution. *Nature*, **289**, 358–362.

OHNENSTETTER, D. & PIANTONE, P. 1992. Pyrochlore-group minerals in the Beauvoir peraluminous leucogranite, Massif Central, France. *Canadian Mineralogist*, **30**, 771–784.

OVERSBY, V. M. & RINGWOOD, A. E. 1981. Lead isotopic studies of zirconolite and perovskite and their implications for long range synroc stability. *Radioactive Waste Management*, **1**, 289–307.

PAN, Y. 1997. Zircon- and monazite-forming metamorphic reactions at Manitouwadge, Ontario. *Canadian Mineralogist*, **35**, 105–118.

PHAM, D. K., MYHRA, S. & TURNER, P. S. 1994. The surface reactivity of hollandite in aqueous solution. *Journal of Materials Research*, **9**, 3174–3181.

PHAM, D. K., NEALL, F. B., MYHRA, S., SMART, R. ST. C. & TURNER, P. S. 1989. Dissolution mechanisms of

$CaTiO_3$ – solution analysis, surface analysis and electron microscope studies – implications for Synroc. *In*: LUTZE, W. & EWING, R. C. (eds) Scientific Basis for Nuclear Waste Management XII. *Materials Research Society Symposium Proceedings*, **127**, 231–240.

POST, J. E., VON DREELE, R. B. & BUSECK, P. R. 1982. Symmetry and cation displacements in hollandites: structure refinements of hollandite, cryptomelane and priderite. *Acta Crystallographica*, **B38**, 1056–1065.

PUTNAM, R. L., NAVROTSKY, A., WOODFIELD, B. F., BOERIO-GOATES, J. & SHAPIRO, J. L. 1999. Thermodynamics of formation for zirconolite ($CaZrTi_2O_7$) from T = 298.15 K to T = 1500 K. *Journal of Chemical Thermodynamics*, **31**, 229–243.

REEVE, K. D., LEVINS, D. M., SEATONBERRY, B. W., RYAN, R. K., HART, K. P. & STEVENS, G. T. 1989. Fabrication and leach testing of synroc containing actinides and fission products. *In*: LUTZE, W. & EWING, R. C. (eds) Scientific Basis for Nuclear Waste Management XII. *Materials Research Society Symposium Proceedings*, **127**, 223–230.

RINGWOOD, A. E., KESSON, S. E., REEVE, K. D., LEVINS, D. M. & RAMM, E. J. 1988. Synroc. *In*: LUTZE, W. & EWING, R. C. (eds) *Radioactive Waste Forms for the Future*. North-Holland, Amsterdam, 233–334.

ROBERTS, S. K., BOURCIER, W. L. & SHAW, H. F. 2000. Aqueous dissolution kinetics of pyrochlore, zirconolite and brannerite at 25, 50, and 75 °C. *Radiochimica Acta*, **88**, 539–543.

SHOUP, S. S., BAMBERGER, C. E., HAVERLOCK, T. J. & PETERSON, J. R. 1997. Aqueous leachability of lanthanide and plutonium titanates. *Journal of Nuclear Materials*, **240**, 112–117.

SINCLAIR, W. & EGGLETON, R. A. 1982. Structure refinement of zirkelite from Kaiserstuhl, West Germany. *American Mineralogist*, **67**, 615–620.

SINCLAIR, W. & MCLAUGHLIN, G. M. 1982. Structure refinement of priderite. *Acta Crystallographica*, **B38**, 245–246.

SMITH, K. L. & LUMPKIN, G. R. 1993. Structural features of zirconolite, hollandite and perovskite, the major waste-bearing phases in synroc. *In*: BOLAND, J. N. & FITZ GERALD, J. D. (eds) *Defects and Processes in the Solid State: Geoscience Applications, The McLaren Volume*. Elsevier, Amsterdam, 401–422.

SMITH, K. L., ZALUZEC, N. J. & LUMPKIN, G. R. 1998. In situ studies of ion irradiated zirconolite, pyrochlore and perovskite. *Journal of Nuclear Materials*, **250**, 36–52.

SMITH, K. L., HART, K. P., LUMPKIN, G. R., MCGLINN, P., LAM, P. & BLACKFORD, M. G. 1991. A description of the kinetics and mechanisms which control the release of HLW elements from synroc. *In*: ABRAJANO, T., JR. & JOHNSON, L. H. (eds) Scientific Basis for Nuclear Waste Management XIV. *Materials Research Society Symposium Proceedings*, **212**, 167–174.

SMITH, K. L., LUMPKIN, G. R., BLACKFORD, M. G., DAY, R. A. & HART, K. P. 1992. The durability of Synroc. *Journal of Materials Research*, **190**, 287–294.

SMITH, K. L., BLACKFORD, M. G., LUMPKIN, G. R., HART, K. P. & ROBINSON, B. J. 1996. Neptunium-doped Synroc: partitioning, leach data and secondary phase development. *In*: MURPHY, W. M. & KNECHT, D. A. (eds) Scientific Basis for Nuclear Waste Management XIX. *Materials Research Society Symposium Proceedings*, **412**, 313–319.

SMITH, K. L., COLELLA, M. *et al.* 1997*a*. Dissolution of Synroc in deionised water at 150 °C. *In*: GRAY, W. J. & TRIAY, R. (eds) Scientific Basis for Nuclear Waste Management XX. *Materials Research Society Symposium Proceedings*, **465**, 349–354.

SMITH, K. L., LUMPKIN, G. R., BLACKFORD, M. G., HAMBLEY, M., DAY, R. A., HART, K. P. & JOSTSONS, A. 1997*b*. Characterisation and leaching behavior of plutonium-bearing Synroc-C. *In*: GRAY, W. J. & TRIAY, R. (eds) Scientific Basis for Nuclear Waste Management XX. *Materials Research Society Symposium Proceedings*, **465**, 1267–1272.

SOLOMAH, A. G. & MATZKE, HJ. 1989. Leaching studies of synroc crystalline ceramic waste forms. *In*: LUTZE, W. & EWING, R. C. (eds) Scientific Basis for Nuclear Waste Management XII. *Materials Research Society Symposium Proceedings*, **127**, 241–248.

STEFANOVSKY, S. V., YUDINTSEV, S. V., GIERÉ, R. & LUMPKIN, G. R. 2004. Nuclear waste forms. *In*: GIERÉ, R. & STILLE, P. (eds) *Energy, Waste, and the Environment: a Geochemical Perspective*. Geological Society, London, Special Publications, **236**, 37–63.

STEWART, M. W. A., BEGG, B. D. *et al.* 2003. Ion irradiation damage in zirconate and titanate ceramics for plutonium disposition. *Proceedings of ICEM '03: The 9th International Conference on Radioactive Waste Management and Environmental Remediation*, in press.

SUBRAMANIAN, M. A., ARAVAMUDAN, G. & SUBBA RAO, G. V. 1983. Oxide pyrochlores – a review. *Progress in Solid State Chemistry*, **15**, 55–143.

SZYMAŃSKI, J. T. & SCOTT, J. D. 1982. A crystal structure refinement of synthetic brannerite, UTi_2O_6, and its bearing on rate of alkaline-carbonate leching of brannerite in ore. *Canadian Mineralogist*, **20**, 271–279.

TROCELLIER, P. 2000. Immobilisation of radionuclides in single-phase crystalline waste forms: a review on their intrinsic properties and long term behaviour. *Ann. Chim. Sci. Mat.*, **25**, 321–337.

TROCELLIER, P. 2001. Chemical durability of high level nuclear waste forms. *Ann. Chim. Sci. Mat.*, **26**, 113–130.

TURNER, P. S., JONES, C. F., MYHRA, S., NEALL, F. B., PHAM, D. K. & SMART, R. ST. C. 1989. Dissolution mechanisms of oxides and titantate cermics – electron microscope and surface analytical studies. *In*: DUFOUR, L.-C., MONTY, C. & PETOT-ERVAS, G. (eds) *Surfaces and Interfaces of Ceramic*

Materials. Kluwer Academic Publishers, Dordrecht, 663–690.

VANCE, E. R. 1994. Synroc: a suitable waste form for actinides. *Materials Research Society Bulletin*, **XIX**, 28–32.

VANCE, E. R., WATSON, J. N. *et al.* 2000. Crystal chemistry, radiation effects and aqueous leaching of brannerite, UTi_2O_6. *Ceramic Transactions*, **107**, 561–568.

WALL, F., WILLIAMS, C. T. & WOOLLEY, A. R. 1999. Pyrochlore in niobium ore deposits. *In*: STANLEY, C. J. (ed) *Mineral Deposits: Processes to Processing*. Balkema Publishers, Rotterdam, Vol. 1, 687–690.

WALL, F., WILLIAMS, C. T., WOOLLEY, A. R. & NASRAOUI, M. 1996. Pyrochlore from weathered carbonatite at Lueshe, Zaire. *Mineralogical Magazine*, **60**, 731–750.

WEBER, W. J., WALD, J. W. & MATZKE, HJ. 1986. Effects of self-radiation damage in Cm-doped $Gd_2Ti_2O_7$ and $CaZrTi_2O_7$. *Journal of Nuclear Materials*, **138**, 196–209.

WEBER, W. J., EWING, R. C. *et al.* 1998. Radiation effects in crystalline ceramics for the immmobilization of high-level nuclear waste and plutonium. *Journal of Materials Research*, **13**, 1434–1484.

WILLIAMS, C. T., WALL, F., WOOLLEY, A. R. & PHILLIPO, S. 1997. Compositional variation in pyrochlore from the Bingo carbonatite, Zaire. *Journal of African Earth Sciences*, **25**, 137–145.

WILLIAMS, C. T., BULAKH, A. G., GIERÉ, R., LUMPKIN, G. R. & MARIANO, A. N. 2001. Alteration features in natural zirconolites from carbonatites. *In*: HART, K. P. & LUMPKIN, G. R. (eds) Scientific Basis for Nuclear Waste Management XXIV. *Materials Research Society Symposium Proceedings*, **663**, 945–952.

WISE, M. A. & ČERNÝ, P. 1990. Primary compositional range and alteration trends of microlite from the Yellowknife pegmatite field, Northwest Territories, Canada. *Mineralogy and Petrology*, **43**, 83–98.

ZHANG, Y., HART, K. P. *et al.* 2001*a*. Durabilities of pyrochlore ceramics designed for the immobilisation of surplus plutonium. *In*: HART, K. P. & LUMPKIN, G. R. (eds) Scientific Basis for Nuclear Waste Management XXIV. *Materials Research Society Symposium Proceedings*, **663**, 325–332.

ZHANG, Y., HART, K. P. *et al.* 2001*b*. Kinetics of uranium release from Synroc phases. *Journal of Nuclear Materials*, **289**, 254–262.

ZHANG, Y., THOMAS, B. S., LUMPKIN, G. R., BLACKFORD, M., ZHANG, Z., COLELLA, M. & ALY, Z. 2003. Dissolution of synthetic brannerite in acidic and alkaline fluids. *Journal of Nuclear Materials*, **321**, 1–7.